NASA TECHNICAL NOTE

NASA TN D-8195

NUMERICAL SOLUTION OF SUPERSONIC THREE-DIMENSIONAL FREE-MIXING FLOWS USING THE PARABOLIC-ELLIPTIC NAVIER-STOKES EQUATIONS

Richard S. Hirsh

Langley Research Center
Hampton, Va. 23665

NATIONAL AERONAUTICS AND SPACE ADMINISTRATION • WASHINGTON, D. C. • NOVEMBER 1976

1. Report No.	2. Government Accession No.	3. Recipient's Catalog No.
NASA TN D-8195		

4. Title and Subtitle	5. Report Date
NUMERICAL SOLUTION OF SUPERSONIC THREE-DIMENSIONAL FREE-MIXING FLOWS USING THE PARABOLIC-ELLIPTIC NAVIER-STOKES EQUATIONS	November 1976
	6. Performing Organization Code
7. Author(s)	8. Performing Organization Report No.
Richard S. Hirsh	L-10750
	10. Work Unit No.
9. Performing Organization Name and Address	505-06-11-03
NASA Langley Research Center	11. Contract or Grant No.
Hampton, VA 23665	
	13. Type of Report and Period Covered
12. Sponsoring Agency Name and Address	Technical Note
National Aeronautics and Space Administration	14. Sponsoring Agency Code
Washington, DC 20546	

15. Supplementary Notes

16. Abstract

A numerical method is presented for solving the parabolic-elliptic Navier-Stokes equations. The solution procedure is applied to three-dimensional supersonic laminar jet flow issuing parallel with a supersonic free stream. A coordinate transformation is introduced which maps the boundaries at infinity into a finite computational domain in order to eliminate difficulties associated with the imposition of free-stream boundary conditions.

Results are presented for an approximate circular jet, a square jet, varying aspect ratio rectangular jets, and interacting square jets. The solution behavior varies from axisymmetric to nearly two-dimensional in character. For cases where comparisons of the present results with those obtained from shear layer calculations could be made, agreement was good.

17. Key Words (Suggested by Author(s))	18. Distribution Statement
Navier-Stokes equations Finite difference Compressible flow Viscous flow Supersonic flow	Unclassified – Unlimited Subject Category 34

19. Security Classif. (of this report)	20. Security Classif. (of this page)	21: No. of Pages	22. Price*
Unclassified	Unclassified	62	$4.25

*For sale by the National Technical Information Service, Springfield, Virginia 22161

CONTENTS

NUMERICAL SOLUTION OF SUPERSONIC THREE-DIMENSIONAL FREE-MIXING FLOWS USING THE PARABOLIC-ELLIPTIC NAVIER-STOKES EQUATIONS

Richard S. Hirsh
Langley Research Center

SUMMARY

A numerical method is presented for solving the parabolic-elliptic Navier-Stokes equations. The solution procedure is applied to three-dimensional supersonic laminar jet flow issuing parallel with a supersonic free stream. A coordinate transformation is introduced which maps the boundaries at infinity into a finite computational domain in order to eliminate difficulties associated with the imposition of free-stream boundary conditions.

Results are presented for an approximate circular jet, a square jet, varying aspect ratio rectangular jets, and interacting square jets. The solution behavior varies from axisymmetric to nearly two-dimensional in character. For cases where comparisons of the present results with those obtained from shear layer calculations could be made, agreement was good.

INTRODUCTION

Free jet and wake flows are common aerodynamic phenomena. These flows are generally turbulent, and the calculation of two-dimensional or axisymmetric turbulent free jets or wakes is difficult (ref. 1) because of problems associated with turbulence modeling; higher order modeling (Reynolds stress equations) is necessary in many cases. For three-dimensional flows with two essential cross-plane velocities, very few calculations have been made. To assess the modeling procedures for three-dimensional flows, it is necessary to develop a numerical procedure for laminar flows, preferably in primitive variables, to allow ease of incorporation of the turbulence models. The purpose of this paper is to present such a procedure and demonstrate its applicability.

The calculation of free-mixing flows has, in the past, been accomplished through use of the boundary-layer assumptions in the two-dimensional or axisymmetric Navier-Stokes equations. The accuracy and validity of these procedures have been well documented in the literature. (See refs. 1 and 2.) However, there are numerous situations where the

flow cannot be considered either two-dimensional or axisymmetric. Jets issuing from rectangular orifices, wakes behind any but the simplest bodies, and the flow downstream of a wing tip are examples of three-dimensional free-mixing flows where boundary-layer assumptions are invalid. The characteristic feature of these flows is the importance of diffusion in two spatial coordinates.

These flows have certain characteristics which are common to boundary-layer flows; for example, the velocities in the plane normal to the main-stream direction are usually much smaller than the main-flow velocity. Also, one expects gradients that exist in the cross directions to be larger than the gradients in the main-flow direction. Therefore, it might be reasonable to use a boundary-layer scaling on the Navier-Stokes equations to effect some simplification; however, this procedure yields an inconsistent set of equations. To lowest order, the cross-stream momentum equations reduce to statements that the pressure is constant, and the resulting number of equations is not sufficient to determine the remaining unknown quantities. A set of equations which is a higher order approximation to the Navier-Stokes than the boundary-layer equations, the parabolic-elliptic Navier-Stokes (PENS) equations, is necessary to overcome this difficulty.

The PENS equations were originally derived (in two dimensions) in reference 3 for the merged flow region near the leading edge of a flat plate in hypersonic flow. An explicit finite-difference method was used to integrate the equations in the domain between the flat plate and the free-stream flow beyond the merged shock layer. The three-dimensional equations are given in reference 4 where the leading-edge flow on a finite-width flat plate is calculated. The alternating direction implicit (ADI) method, introduced in reference 5, is used to solve the equations. The two- and three-dimensional problems are reviewed in reference 6 where a new predictor-corrector method is presented as the most appropriate one to use. See also reference 7 for further details. This analysis has been extended to the hypersonic tip region of a cone in reference 8.

The flow past a cone received further study in references 9 and 10 where the PENS equations were used to calculate the entire flow field between a well defined shock envelope and the cone surface. The equations solved in references 9 and 10 are very similar to those of reference 8, but the arguments leading to their derivation are somewhat different. A fully implicit numerical method is used to solve the resulting equations between the body and the shock, where the Rankine-Hugoniot equations are imposed.

The PENS concepts have also been utilized in subsonic, incompressible flows for internal (ref. 11) and external (ref. 12) cases. However, the need to solve a Poisson equation for the cross-plane pressure in these incompressible flows separates them from the procedures used in references 3, 4, and 6 to 10 and the present work where only supersonic flows are considered.

The present work solves the parabolic-elliptic Navier-Stokes equations for supersonic free-mixing flows. It is found necessary to incorporate a coordinate transformation into the PENS equations in order to impose free-stream boundary conditions on the flow. The character of the equations is such that they are well suited to solution by the ADI method. This finite-difference method generates block tridiagonal matrix equations which allow for the simultaneous solution of all the variables at each location. Preliminary results from this investigation were given in reference 13. Further test cases and discussion of results are presented in this paper.

This solution procedure of the PENS system is applied to three-dimensional, supersonic, rectangular jet flows in which the jet aspect ratio is varied from one (square jet) to large values representative of slits (two-dimensional jets). Various combinations of free-stream Mach and Reynolds numbers are studied. Whenever possible, results from free shear layer calculations obtained by using the boundary-layer approximations are compared with those obtained by using the PENS equations. The range of applicability of the procedure is demonstrated from the near axisymmetry of the square, through a true three-dimensional region of moderate aspect ratios, to a quasi-two-dimensional flow in the high-aspect-ratio limit which approximates a two-dimensional jet.

Finally, a test case corresponding to interacting jet flow behind an aircraft was computed. No difficulties were encountered during the course of these calculations which gave the correct qualitative results. No quantitative comparisons could be made with any two-dimensional or axisymmetric shear-layer predictions since this flow is three-dimensional, and beyond the scope of boundary-layer theory.

SYMBOLS

A, B	transformation constants
$[A], [B], [C]$	matrices defined by equation (23)
a, b, c	components of matrices $[A], [B], [C]$
a, b, α	coefficients in equation (A1)
C_p	specific heat
$\vec{D}$	vector defined by equation (23)
$\frac{D}{Dt}$	convective derivative

d	component of vector $\vec{D}$
h	width of unit jet (reference length)
L_r	reference length
M	Mach number
N_{Pr}	Prandtl number
N_{Re}	Reynolds number
p	pressure
Q	any representative dependent variable
S	$= S^*/T_r$
S^*	Sutherland's constant
T	temperature
u,v,w	component velocities in x-, y-, and z-directions, respectively
$\vec{W}$	vector of dependent variables (see eq. (24))
x,y,z	coordinate directions
γ	ratio of specific heats
Δ	dilatation
$\Delta x, \Delta y, \Delta z$	grid spacings in x-, y-, and z-directions, respectively
$\Delta\eta, \Delta\zeta$	grid spacings in η- and ζ-directions, respectively
δ	central difference operator; also measure of boundary-layer scale
η, ζ	transformed y- and z-coordinates

μ viscosity

ξ streamwise coordinate in transformed plane

ρ density

Φ dissipation

Superscripts:

i discretized x-position

* intermediate step of alternating direction implicit method

T transpose

Subscripts:

j,k discretized y- and z-positions, respectively

r reference quantity

∞ free stream

+,- upper and lower grid spacings used with nonuniform grid

ℓ center line

A bar over a symbol denotes a nondimensional quantity.

GOVERNING EQUATIONS

The Navier-Stokes equations for the steady, three-dimensional flow of a viscous, heat-conducting fluid are, in Cartesian coordinates

for x-momentum,

$$\rho \frac{Du}{Dt} = -\frac{\partial p}{\partial x} + \frac{\partial}{\partial x}\left[\mu\left(2\frac{\partial u}{\partial x} - \frac{2}{3}\Delta\right)\right] + \frac{\partial}{\partial y}\left[\mu\left(\frac{\partial u}{\partial y} + \frac{\partial v}{\partial x}\right)\right] + \frac{\partial}{\partial z}\left[\mu\left(\frac{\partial w}{\partial x} + \frac{\partial u}{\partial z}\right)\right] \quad (1)$$

for y-momentum,

$$\rho \frac{Dv}{Dt} = -\frac{\partial p}{\partial y} + \frac{\partial}{\partial x}\left[\mu\left(\frac{\partial u}{\partial y} + \frac{\partial v}{\partial x}\right)\right] + \frac{\partial}{\partial y}\left[\mu\left(2\,\frac{\partial v}{\partial y} - \frac{2}{3}\Delta\right)\right] + \frac{\partial}{\partial z}\left[\mu\left(\frac{\partial v}{\partial z} + \frac{\partial w}{\partial y}\right)\right] \tag{2}$$

for z-momentum,

$$\rho \frac{Dw}{Dt} = -\frac{\partial p}{\partial z} + \frac{\partial}{\partial x}\left[\mu\left(\frac{\partial w}{\partial x} + \frac{\partial u}{\partial z}\right)\right] + \frac{\partial}{\partial y}\left[\mu\left(\frac{\partial v}{\partial z} + \frac{\partial w}{\partial y}\right)\right] + \frac{\partial}{\partial z}\left[\mu\left(2\,\frac{\partial w}{\partial z} - \frac{2}{3}\Delta\right)\right] \tag{3}$$

and for energy,

$$\rho C_p \frac{DT}{Dt} = \frac{Dp}{Dt} + \frac{C_p}{N_{Pr}}\left[\frac{\partial}{\partial x}\left(\mu\,\frac{\partial T}{\partial x}\right) + \frac{\partial}{\partial y}\left(\mu\,\frac{\partial T}{\partial y}\right) + \frac{\partial}{\partial z}\left(\mu\,\frac{\partial T}{\partial z}\right)\right] + \mu\Phi. \tag{4}$$

where

$$\Phi = 2\left[\left(\frac{\partial u}{\partial x}\right)^2 + \left(\frac{\partial v}{\partial y}\right)^2 + \left(\frac{\partial w}{\partial z}\right)^2\right] + \left(\frac{\partial v}{\partial x} + \frac{\partial u}{\partial y}\right)^2 + \left(\frac{\partial w}{\partial y} + \frac{\partial v}{\partial z}\right)^2 + \left(\frac{\partial u}{\partial z} + \frac{\partial w}{\partial x}\right)^2 - \frac{2}{3}\left(\frac{\partial u}{\partial x} + \frac{\partial v}{\partial y} + \frac{\partial w}{\partial z}\right)^2$$

$$\Delta = \frac{\partial u}{\partial x} + \frac{\partial v}{\partial y} + \frac{\partial w}{\partial z}$$

$$\frac{D}{Dt} = u\,\frac{\partial}{\partial x} + v\,\frac{\partial}{\partial y} + w\,\frac{\partial}{\partial z}$$

and the continuity equation is

$$\frac{\partial}{\partial x}(\rho u) + \frac{\partial}{\partial y}(\rho v) + \frac{\partial}{\partial z}(\rho w) = 0 \tag{5}$$

The elliptic nature of these equations makes it necessary, for a numerical solution, to store the unknowns for the entire three-dimensional region being computed. The core storage available on present computers is insufficient to practicably handle any but the coarsest grids, which yield computed results of very low accuracy. Thus, methods to reduce the equations to a form more tractable for computations must be employed.

Boundary-Layer Approximation

The obvious simplification to be tried, for viscous flows with a dominant flow direction, is the classical boundary-layer technique which scales the various field quantities and their gradients according to their relative sizes. This approximation will be seen to be invalid for three-dimensional flows where, as assumed below, the cross-plane

velocities and characteristic length scales are of the same order of magnitude, but not necessarily equal.

If the x-direction is assumed to be the dominant direction of flow, and the main changes in the flow field are taken to occur perpendicular to this main stream, that is, in the YZ plane, the boundary-layer scaling for the equations is

$$\bar{u} = \frac{u}{u_r} \qquad \bar{v} = \frac{v}{\delta u_r} \qquad \bar{w} = \frac{w}{\delta u_r}$$

$$\bar{x} = \frac{x}{L_r} \qquad \bar{y} = \frac{y}{\delta L_r} \qquad \bar{z} = \frac{z}{\delta L_r}$$

$$\bar{p} = \frac{p}{\rho_r u_r^2} \qquad \bar{\rho} = \frac{\rho}{\rho_r} \qquad \bar{\mu} = \frac{\mu}{\mu_r}$$

where

$$\delta = \frac{1}{\sqrt{N_{Re}}}$$

$$N_{Re} = \frac{\rho_r u_r L_r}{\mu_r}$$

Placing this scaling into equations (1) to (4) gives (after dropping the overbar)

$$\rho \frac{Du}{Dt} = -\frac{\partial p}{\partial x} + \frac{1}{N_{Re}} \frac{\partial}{\partial x}\left[\mu\left(2 \frac{\partial u}{\partial x} - \frac{2}{3}\Delta\right)\right] + \frac{\partial}{\partial y}\left[\mu\left(\frac{\partial u}{\partial y} + \frac{1}{N_{Re}} \frac{\partial v}{\partial x}\right)\right] + \frac{\partial}{\partial z}\left[\mu\left(\frac{1}{N_{Re}} \frac{\partial w}{\partial x} + \frac{\partial u}{\partial z}\right)\right]$$

$$\rho \frac{Dv}{Dt} = -N_{Re} \frac{\partial p}{\partial y} + \frac{\partial}{\partial x}\left[\mu\left(\frac{\partial u}{\partial y} + \frac{1}{N_{Re}} \frac{\partial v}{\partial x}\right)\right] + \frac{\partial}{\partial y}\left[\mu\left(2 \frac{\partial v}{\partial y} - \frac{2}{3}\Delta\right)\right] + \frac{\partial}{\partial z}\left[\mu\left(\frac{\partial v}{\partial z} + \frac{\partial w}{\partial y}\right)\right]$$

$$\rho \frac{Dw}{Dt} = -N_{Re} \frac{\partial p}{\partial z} + \frac{\partial}{\partial x}\left[\mu\left(\frac{1}{N_{Re}} \frac{\partial w}{\partial x} + \frac{\partial u}{\partial z}\right)\right] + \frac{\partial}{\partial y}\left[\mu\left(\frac{\partial v}{\partial x} + \frac{\partial w}{\partial y}\right)\right] + \frac{\partial}{\partial z}\left[\mu\left(2 \frac{\partial w}{\partial z} - \frac{2}{3}\Delta\right)\right]$$

$$\frac{\partial}{\partial x}(\rho u) + \frac{\partial}{\partial y}(\rho v) + \frac{\partial}{\partial z}(\rho w) = 0$$

where the energy equation has been omitted since it adds nothing to the following argument concerning the momentum equations. Making the boundary-layer approximation by retaining only the highest order terms in the Reynolds number gives

$$\rho \frac{Du}{Dt} = -\frac{\partial p}{\partial x} + \frac{\partial}{\partial y}\left[\mu\left(\frac{\partial u}{\partial y}\right)\right] + \frac{\partial}{\partial z}\left[\mu\left(\frac{\partial u}{\partial z}\right)\right]$$

$$\frac{\partial p}{\partial y} = 0$$

$$\frac{\partial p}{\partial z} = 0$$

$$\frac{\partial}{\partial x}(\rho u) + \frac{\partial}{\partial y}(\rho v) + \frac{\partial}{\partial z}(\rho w) = 0$$

Hence, the two cross momentum equations have degenerated into a statement that the pressure is constant in cross planes and the system of equations which results is not sufficient to determine all the unknowns. This condition was noted previously by Greber in a comment following an article by Pai and Hsieh (ref. 14) who used an a priori boundary-layer scaling on equations similar to equations (1) to (3). Hence, a true boundary-layer scaling cannot be expected to yield one simple set of equations which can be easily solved and a different approximation must be made.

Parabolic-Elliptic Navier-Stokes Equations

Although a strict application of boundary-layer scaling is abandoned, some of the concepts from the boundary-layer theory indicate a means to simplify the equations. The only assumption which can be made is the predominance of the convection in the one main-flow direction over the shear stress in this direction. This assumption leads to the (Reynolds number dependent) conclusion that x-derivatives associated with the shear stress can be neglected. With the x-direction taken to be the convective main-stream direction, the Navier-Stokes equations, after neglecting all x-derivatives associated with shear, become

$$\rho \frac{Du}{Dt} = -\frac{\partial p}{\partial x} + \frac{\partial}{\partial y}\left[\mu\left(\frac{\partial u}{\partial y}\right)\right] + \frac{\partial}{\partial z}\left[\mu\left(\frac{\partial u}{\partial z}\right)\right] \tag{6}$$

$$\rho \frac{Dv}{Dt} = -\frac{\partial p}{\partial y} + \frac{\partial}{\partial y}\left[\frac{2}{3}\mu\left(2\frac{\partial v}{\partial y} - \frac{\partial w}{\partial z}\right)\right] + \frac{\partial}{\partial z}\left[\mu\left(\frac{\partial v}{\partial z}\right)\right] \tag{7}$$

$$\rho \frac{Dw}{Dt} = -\frac{\partial p}{\partial z} + \frac{\partial}{\partial y}\left[\mu\left(\frac{\partial w}{\partial y}\right)\right] + \frac{\partial}{\partial z}\left[\frac{2}{3}\mu\left(2\frac{\partial w}{\partial z} - \frac{\partial v}{\partial y}\right)\right] \tag{8}$$

The x-momentum equation is the same as would have been produced by a true boundary-layer scaling, but since no quantitative assumptions have been made concerning the relative sizes of the x-, y-, or z-derivatives, the y- and z-momentum equations are retained, although in somewhat simpler form than equations (2) and (3). The continuity equation remains unchanged, that is, equation (5). With the same arguments, the energy equation becomes

$$\rho C_p \frac{DT}{Dt} = \frac{Dp}{Dt} + \frac{C_p}{N_{Pr}}\left\{\frac{\partial}{\partial y}\left[\mu\left(\frac{\partial T}{\partial y}\right)\right] + \frac{\partial}{\partial z}\left[\mu\left(\frac{\partial T}{\partial z}\right)\right]\right\} + \mu\Phi \tag{9}$$

where

$$\Phi = \left(\frac{\partial u}{\partial y}\right)^2 + \left(\frac{\partial u}{\partial z}\right)^2 + \frac{4}{3}\left[\left(\frac{\partial v}{\partial y}\right)^2 - \left(\frac{\partial v}{\partial y}\right)\left(\frac{\partial w}{\partial z}\right) + \left(\frac{\partial w}{\partial z}\right)^2\right] + \left(\frac{\partial w}{\partial y}\right)^2 + 2\left(\frac{\partial w}{\partial y}\right)\left(\frac{\partial v}{\partial z}\right) + \left(\frac{\partial v}{\partial z}\right)^2$$

When these equations are supplemented by an equation of state and a viscosity relation

$$p = \rho RT$$

$$\frac{\mu}{\mu_r} = \left(\frac{T_r + S^*}{T + S^*}\right)\left(\frac{T}{T_r}\right)^{3/2}$$

where R is the gas constant, a system of five equations for five unknowns is obtained after elimination of the density by the perfect gas equation of state.

The elliptic nature of the Navier-Stokes equations in the x-direction has thus been eliminated; consequently, the equations are parabolic in x and marching integration may be used in the streamwise direction. This simplification significantly reduces the computational requirements since it eliminates the need to store all the field quantities at each x-location and results in a substantial reduction in computer storage. Thus, they are given the name parabolic-elliptic Navier-Stokes equations, since the assumptions allow a march in x away from an initial data plane and yet retain the elliptic character of the crossflow planes (YZ planes) due to the inclusion of all second derivatives in y and z. For example, flows with swirl or possible crossflow recirculation (vortices) in the YZ planes can be computed. Only reverse flow in the main-stream direction is precluded because of the parabolic marching nature of the solution procedure in this direction.

The pressure can be advanced by rewriting the x-derivative in the continuity equation as follows:

$$(\rho u)_x = \left(\frac{pu}{T}\right)_x = \frac{u}{T} p_x + \frac{p}{T} u_x - \frac{pu}{T^2} T_x$$

The p_x term can be used to march to the next station. There is no explicit viscous term present and any dissipation which may tend to damp pressure oscillations must come through a coupling with the other field quantities present in the continuity equation.

If equations (5) to (9) are cast in nondimensional form by using free-stream values of u_∞, p_∞, and T_∞, and the minimum initial jet width h as the reference length, the nondimensional equations become

for x-momentum,

$$\rho \frac{Du}{Dt} = -\frac{1}{\gamma M_\infty^2} \frac{\partial p}{\partial x} + \frac{1}{N_{Re}} \left\{ \frac{\partial}{\partial y} \left[\mu \left(\frac{\partial u}{\partial y} \right) \right] + \frac{\partial}{\partial z} \left[\mu \left(\frac{\partial u}{\partial z} \right) \right] \right\} \tag{10}$$

for y-momentum,

$$\rho \frac{Dv}{Dt} = -\frac{1}{\gamma M_\infty^2} \frac{\partial p}{\partial y} + \frac{1}{N_{Re}} \left\{ \frac{2}{3} \frac{\partial}{\partial y} \left[\mu \left(2 \frac{\partial v}{\partial y} - \frac{\partial w}{\partial z} \right) \right] + \frac{\partial}{\partial z} \left[\mu \left(\frac{\partial v}{\partial z} + \frac{\partial w}{\partial y} \right) \right] \right\} \tag{11}$$

for z-momentum,

$$\rho \frac{Dw}{Dt} = -\frac{1}{\gamma M_\infty^2} \frac{\partial p}{\partial z} + \frac{1}{N_{Re}} \left\{ \frac{\partial}{\partial y} \left[\mu \left(\frac{\partial v}{\partial x} + \frac{\partial w}{\partial y} \right) \right] + \frac{2}{3} \frac{\partial}{\partial z} \left[\mu \left(2 \frac{\partial w}{\partial z} - \frac{\partial v}{\partial y} \right) \right] \right\} \tag{12}$$

for energy,

$$\rho \frac{DT}{Dt} = \left(\frac{\gamma - 1}{\gamma} \right) \frac{Dp}{Dt} + \frac{1}{N_{Pr} R} \left\{ \frac{\partial}{\partial y} \left[\mu \left(\frac{\partial T}{\partial y} \right) \right] + \frac{\partial}{\partial z} \left[\mu \left(\frac{\partial T}{\partial z} \right) \right] \right\} + \frac{\gamma - 1}{R} M_\infty^2 \mu \left\{ \left(\frac{\partial u}{\partial y} \right)^2 + \left(\frac{\partial u}{\partial z} \right)^2 \right.$$

$$\left. + \frac{4}{3} \left[\left(\frac{\partial v}{\partial y} \right)^2 - \left(\frac{\partial v}{\partial y} \right) \left(\frac{\partial w}{\partial z} \right) + \left(\frac{\partial w}{\partial z} \right) \right]^2 + \left(\frac{\partial w}{\partial y} \right)^2 + 2 \left(\frac{\partial w}{\partial y} \right) \left(\frac{\partial v}{\partial z} \right) + \left(\frac{\partial v}{\partial z} \right)^2 \right\} \tag{13}$$

for continuity,

$$\frac{\partial}{\partial x}(\rho u) + \frac{\partial}{\partial y}(\rho v) + \frac{\partial}{\partial z}(\rho w) = 0 \tag{14}$$

for the equation of state,

$$p = \rho T$$

and for Sutherland's law,

$$\mu = \left(\frac{1 + S}{T + S} \right) T^{3/2}$$

These nondimensional equations are to be solved subject to the following boundary conditions:

$$y,z \to \infty: \quad u = 1; \quad v = w = 0; \quad T = 1; \quad p = 1$$

$$y = 0: \quad \frac{\partial u}{\partial y} = 0; \quad v = 0; \quad \frac{\partial w}{\partial y} = 0; \quad \frac{\partial T}{\partial y} = 0; \quad \frac{\partial p}{\partial y} = 0$$

$$z = 0: \quad \frac{\partial u}{\partial z} = 0; \quad \frac{\partial v}{\partial z} = 0; \quad w = 0; \quad \frac{\partial T}{\partial z} = 0; \quad \frac{\partial p}{\partial z} = 0$$

and initial conditions specifying the particular jet flow problem to be investigated.

Equations of this type (eqs. (10) to (14)), where the pressure is computed and not assumed, have been shown to be singular at $M = 1$, if the $\frac{\partial p}{\partial x}$ term is treated implicitly, and singular at $M = 0$, if the pressure gradient is calculated in an explicit manner during a numerical calculation. (See ref. 6.) If the $\frac{\partial p}{\partial x}$ term is neglected entirely or specified from a boundary-layer approximation, then the parabolic march in x can proceed without difficulty. (See ref. 6.)

Thus, since the class of problems chosen to test the overall method should avoid any of these integration difficulties, if possible, equations (10) to (14) will be solved for a supersonic jet issuing into a supersonic free stream. The $M = 0$ behavior takes place near boundaries (where $u = 0$), and therefore, a free jet problem avoids this singular behavior. However, the jet cannot exhaust into an ambient atmosphere since here $u = 0$ also. Thus, a jet issuing into a moving free stream is suitable. To avoid any difficulties at $M = 1$, both streams were chosen to be supersonic.

NUMERICAL PROCEDURE

Integration Technique

An implicit numerical procedure was chosen to solve the governing equations for a number of reasons. The success of implicit methods on the two- and three-dimensional boundary-layer equations implies that they should be efficient for the boundary-layer-like parabolic-elliptic Navier-Stokes equations (eqs. (10) to (14)). It is expected that solutions may be required at large distances downstream from the initial data plane; consequently, large x-steps are desirable. The need to eliminate the step-size restrictions of explicit methods leads to a consideration of unconditionally stable methods which are consistent in their marching variation. The particular implicit method used in this study is the alternating direction implicit (ADI) method of Peaceman and Rachford. (See ref. 5.) The ADI method is ideally suited for the solution of equations (10) to (14). There is no stability restriction on the step size (see appendix A) and hence, large x-steps are permitted. The

method has second-order truncation error in its marching variation, which is also a requirement for the type of flow envisioned, since the x-history of the flow must be traced accurately at each step. Finally, the method does not require the inversion of a sparse-banded matrix as a fully implicit or Crank-Nicolson method would. Simple tridiagonal coefficient matrices which are generated at each step require much less storage and time for their inversion in relation to sparse-banded matrices. The method has previously been shown to be effective for a set of equations similar to those used in the present approach. (See ref. 4.) The use of this technique has also been attempted on the parabolic-elliptic Navier-Stokes equations in cylindrical polar coordinates for the flow over a cone at incidence. (See ref. 10.) The authors of this work state that an ADI procedure was attempted, but failed to work because of difficulties encountered on the azimuthal sweep of the ADI method. It is possible that the nonsymmetry of the crossflow momentum equations in polar coordinates caused the difficulty. Nevertheless, in Cartesian coordinates, equations (10) and (14) are perfectly symmetric in yz and vw, and this objection does not arise.

Coordinate Transformation

Equations (10) to (14) were cast in finite-difference form and solved for the supersonic free jet problem. Major difficulties were encountered because of the imposition of boundary conditions at arbitrary distances into the assumed free stream. The details of these results are discussed in reference 13. The exact asymptotic behavior of the solution was not known; thus, the conditions in the free stream could not be imposed at any particular chosen distance away from the jet orifice since the eventual growth of the jet, as it proceeds downstream in the x-direction, will reach this boundary and make the imposed conditions incompatible with the flow. To remedy this, a coordinate transformation is introduced into equations (10) to (14) which allows conditions at infinity to be imposed at some finite distance in the computational domain. This is accomplished by the transformation

$$\left.\begin{aligned} \eta &= \frac{Ay}{1 + Ay} \\ \zeta &= \frac{Bz}{1 + Bz} \end{aligned}\right\} \tag{15}$$

which maps zero onto zero, and infinity in the physical plane onto unity in the $\eta\zeta$ plane. This linear transformation has been used successfully by other investigators on a variety of problems. (See refs. 15 to 17.) More complicated transformations do exist (refs. 18 and 19), but the transformation (eq. (15)) produced good results; consequently, no others

were tried. With equation (15), the governing equations of the problem to be solved (eqs. (10) to (14)) are (with $\xi = x$) as follows:

$$\rho u u_\xi + \left[\rho v + 2A\mu(1-\eta)\right] A(1-\eta)^2 u_\eta + \left[\rho w + 2B\mu(1-\zeta)\right] B(1-\zeta)^2 u_\zeta$$

$$= -\frac{1}{\gamma M_\infty^2} p_\xi + \frac{1}{N_{Re}}\left[A^2(1-\eta)^4\left(\mu_T T_\eta u_\eta + \mu u_{\eta\eta}\right) + B^2(1-\zeta)^4\left(\mu_T T_\zeta u_\zeta + \mu u_{\zeta\zeta}\right)\right] \qquad (16)$$

$$\rho u v_\xi + \left[\rho v + \frac{8}{3} A\mu(1-\eta)\right] A(1-\eta)^2 v_\eta + \left[\rho w + 2B\mu(1-\zeta)\right] B(1-\zeta)^2 v_\zeta$$

$$= -\frac{1}{\gamma M_\infty^2} A(1-\eta)^2 p_\eta + \frac{1}{N_{Re}}\left\{\frac{4}{3} A^2(1-\eta)^4\left(\mu_T T_\eta v_\eta + \mu v_{\eta\eta}\right) + B^2(1-\zeta)^4\left(\mu_T T_\zeta v_\zeta + \mu v_{\zeta\zeta}\right)\right.$$

$$\left. + AB(1-\eta)^2(1-\zeta)^2\left[\frac{1}{3}\mu w_{\eta\zeta} + \mu_T\left(T_\zeta w_\eta - \frac{2}{3} T_\eta w_\zeta\right)\right]\right\} \qquad (17)$$

$$\rho u w_\xi + \left[\rho v + 2A\mu(1-\eta)\right] A(1-\eta)^2 w_\eta + \left[\rho w + \frac{8}{3} B\mu(1-\zeta)\right] B(1-\zeta)^2 w_\zeta$$

$$= -\frac{1}{\gamma M_\infty^2} B(1-\zeta)^2 p_\zeta + \frac{1}{N_{Re}}\left\{A^2(1-\eta)^4\left(\mu_T T_\eta w_\eta + \mu w_{\eta\eta}\right) + \frac{4}{3} B^2(1-\zeta)^4\left(\mu_T T_\zeta w_\zeta + \mu w_{\zeta\zeta}\right)\right.$$

$$\left. + AB(1-\eta)^2(1-\zeta)^2\left[\frac{1}{3}\mu v_{\eta\zeta} + \mu_T\left(T_\eta v_\zeta - \frac{2}{3} T_\zeta v_\eta\right)\right]\right\} \qquad (18)$$

$$\rho u T_\xi + \left[\rho v + \frac{2\mu}{N_{Pr}} A(1-\eta)\right] A(1-\eta)^2 T_\eta + \left[\rho w + \frac{2\mu}{N_{Pr}} B(1-\zeta)\right] B(1-\zeta)^2 T_\zeta$$

$$= \frac{\gamma - 1}{\gamma}\left[u p_\xi + vA(1-\eta)^2 p_\eta + wB(1-\zeta)^2 p_\zeta\right] + \frac{1}{N_{Pr} N_{Re}}\left[A^2(1-\eta)^4\left(\mu_T T_\eta^2 + \mu T_{\eta\eta}\right)\right.$$

$$\left. + B^2(1-\zeta)^4\left(\mu_T T_\zeta^2 + \mu T_{\zeta\zeta}\right)\right] + \frac{(\gamma-1)M_\infty^2}{N_{Re}}\mu\left[A^2(1-\eta)^4\left(u_\eta^2 + w_\eta^2 + \frac{4}{3} v_\eta^2\right)\right.$$

$$\left. + B^2(1-\zeta)^4\left(u_\zeta^2 + v_\zeta^2 + \frac{4}{3} w_\zeta^2\right) + AB(1-\eta)^2(1-\zeta)^2\left(w_\eta v_\zeta - \frac{4}{3} v_\eta w_\zeta\right)\right] \qquad (19)$$

$$u p_\xi - \rho u T_\xi + p u_\xi + A(1-\eta)^2\left(v p_\eta - \rho v T_\eta + p v_\eta\right) + B(1-\zeta)^2\left(w p_\zeta - \rho w T_\zeta + p w_\zeta\right) = 0 \qquad (20)$$

These equations are subject to the transformed boundary conditions

$$\eta = 1;\quad \zeta = 1:\quad u = 1;\quad v = 0;\quad w = 0;\quad T = 1;\quad p = 1$$

$$\eta = 0:\quad \frac{\partial u}{\partial \eta} = 0;\quad v = 0;\quad \frac{\partial w}{\partial \eta} = 0;\quad \frac{\partial T}{\partial \eta} = 0;\quad \frac{\partial p}{\partial \eta} = 0$$

$$\zeta = 0:\quad \frac{\partial u}{\partial \zeta} = 0;\quad \frac{\partial v}{\partial \zeta} = 0;\quad w = 0;\quad \frac{\partial T}{\partial \zeta} = 0;\quad \frac{\partial p}{\partial \zeta} = 0$$

The ADI procedure is used to difference equations (16) to (20) in x, with the y- and z-derivatives expressed as central differences. As an example, by using the notation

$$\delta_z u^i_{j,k} = \frac{1}{2\Delta\zeta}\left(u^i_{j,k+1} - u^i_{j,k-1}\right) \tag{21a}$$

$$\delta^2_z u^i_{j,k} = \frac{1}{\Delta\zeta^2}\left(u^i_{j,k+1} - 2u^i_{j,k} + u^i_{j,k-1}\right) \tag{21b}$$

the complete differencing scheme for the x-momentum equation is for the first step:

$$(\rho u)^{i+\frac{1}{2}}_{j,k}\left(\frac{u^*_{j,k} - u^i_{j,k}}{\Delta\xi_+/2}\right) + \left[(\rho v)^{i+\frac{1}{2}}_{j,k} + 2A\mu^{i+\frac{1}{2}}_{j,k}\left(1 - \eta_j\right)\right]A\left(1 - \eta_j\right)^2\delta_y u^i_{j,k} + \left[(\rho w)^{i+\frac{1}{2}}_{j,k} + 2B\mu^{i+\frac{1}{2}}_{j,k}\left(1 - \zeta_k\right)\right]B\left(1 - \zeta_k\right)^2\delta_z u^*_{j,k}$$

$$= -\frac{1}{\gamma M^2_\infty}\left(\frac{p^*_{j,k} - p^i_{j,k}}{\Delta\xi_+/2}\right) + \frac{1}{N_{Re}}\left(A^2\left(1 - \eta_j\right)^4\left\{\frac{1}{2}\left(\frac{\partial\mu}{\partial T}\right)^{i+\frac{1}{2}}_{j,k}\left[\left(\frac{\partial T}{\partial \eta}\right)^{i+\frac{1}{2}}_{j,k}\delta_y u^i_{j,k} + \left(\frac{\partial u}{\partial \eta}\right)^{i+\frac{1}{2}}_{j,k}\delta_y T^i_{j,k}\right] + \mu^{i+\frac{1}{2}}_{j,k}\delta^2_y u^i_{j,k}\right\}\right.$$

$$\left. + B^2\left(1 - \zeta_k\right)^4\left\{\frac{1}{2}\left(\frac{\partial\mu}{\partial T}\right)^{i+\frac{1}{2}}_{j,k}\left[\left(\frac{\partial T}{\partial \zeta}\right)^{i+\frac{1}{2}}_{j,k}\delta_z u^*_{j,k} + \left(\frac{\partial u}{\partial \zeta}\right)^{i+\frac{1}{2}}_{j,k}\delta_z T^*_{j,k}\right] + \mu^{i+\frac{1}{2}}_{j,k}\delta^2_z u^*_{j,k}\right\}\right)$$

and for the second step:

$$(\rho u)^{i+\frac{1}{2}}_{j,k}\left(\frac{u^{i+1}_{j,k} - u^*_{j,k}}{\Delta\xi_+/2}\right) + \left[(\rho v)^{i+\frac{1}{2}}_{j,k} + 2A\mu^{i+\frac{1}{2}}_{j,k}\left(1 - \eta_j\right)\right]A\left(1 - \eta_j\right)^2\delta_y u^{i+1}_{j,k} + \left[(\rho w)^{i+\frac{1}{2}}_{j,k} + 2B\mu^{i+\frac{1}{2}}_{j,k}\left(1 - \zeta_k\right)\right]B\left(1 - \zeta_k\right)^2\delta_z u^*_{j,k}$$

$$= -\frac{1}{\gamma M^2_\infty}\left(\frac{p^{i+1}_{j,k} - p^*_{j,k}}{\Delta\xi_+/2}\right) + \frac{1}{N_{Re}}\left(A^2\left(1 - \eta_j\right)^4\left\{\frac{1}{2}\left(\frac{\partial\mu}{\partial T}\right)^{i+\frac{1}{2}}_{j,k}\left[\left(\frac{\partial T}{\partial \eta}\right)^{i+\frac{1}{2}}_{j,k}\delta_y u^{i+1}_{j,k} + \left(\frac{\partial u}{\partial \eta}\right)^{i+\frac{1}{2}}_{j,k}\delta_y T^{i+1}_{j,k}\right] + \mu^{i+\frac{1}{2}}_{j,k}\delta^2_y u^{i+1}_{j,k}\right\}\right.$$

$$\left. + B^2\left(1 - \zeta_k\right)^4\left\{\frac{1}{2}\left(\frac{\partial\mu}{\partial T}\right)^{i+\frac{1}{2}}_{j,k}\left[\left(\frac{\partial T}{\partial \zeta}\right)^{i+\frac{1}{2}}_{j,k}\delta_z u^*_{j,k} + \left(\frac{\partial u}{\partial \zeta}\right)^{i+\frac{1}{2}}_{j,k}\delta_z T^*_{j,k}\right] + \mu^{i+\frac{1}{2}}_{j,k}\delta^2_z u^*_{j,k}\right\}\right).$$

where the product of unknown derivative terms which appear in equation (17) have been averaged to make the sum of the two ADI steps second order accurate about the point $\left(i + \frac{1}{2}\right)$.

The only difficulty arises from the cross derivatives of velocity present in the y- and z-momentum equations. These derivatives cannot be differenced implicitly since the tridiagonal structure of the resulting matrices would be destroyed. These derivatives are treated in the same manner as all the nonlinear coefficients present in the differenced equations.

Linearization Scheme

The ADI procedure is a two-step, second-order-accurate, implicit integration technique. The first step advances the solution from location (i) to an intermediate stage of computation, much like a predictor step; and the second step advances the solution to the new location (i + 1), much like a corrector step. The solution generated is then second order accurate about the point $\left(i + \frac{1}{2}\right)$. (See fig. 1.) This point is not equivalent to the intermediate, *, step of the ADI procedure. Hence, a method must be developed to compute all the nonlinear coefficients (and the cross derivatives) at the $i + \frac{1}{2}$ point. This computation can be accomplished by a quadratic extrapolation from the two previous x-stations i and i - 1 (ref. 4) by use of the predictor-corrector procedure of Douglas and Jones (ref. 20) or by the recursive iteration technique, presented in reference 13, common to many numerical boundary-layer procedures. (See refs. 21 and 22.) This last method consumes a great deal of time (each iteration is equivalent to a full marching step), and it was found that the quadratic extrapolation yielded the same results, although it required slightly more computer storage. Since computer time was a limiting factor in some of the calculations to be presented, all the nonlinear coefficients and cross derivatives were calculated at the $i + \frac{1}{2}$ point by extrapolation by using

$$Q_{j,k}^{i+\frac{1}{2}} = \frac{\left[\frac{1}{2}(\Delta x_+) + (\Delta x_-)\right] Q_{j,k}^{i} - \frac{1}{2}(\Delta x_+) Q_{j,k}^{i-1}}{(\Delta x_-)} \tag{22}$$

where Q refers to any of these quantities, and allowance has been made for variable step size in the x-direction.

Initial and Boundary Conditions

The solution domain for the free jet problems was the semi-infinite quarter plane bounded by the axes of the symmetry of the jet and extending to infinity in both cross directions (y,z) in the actual physical plane. The boundary condition difficulties

encountered when assuming an arbitrary position for the free stream (ref. 13) were overcome by use of the coordinate transformation (eq. (15)). This usage allows imposition of the unknown free-stream conditions at the last computational node, that is, at $\eta = 1$ or $\zeta = 1$. Conditions on the two lines of symmetry present were fixed by setting the velocity normal to the symmetry line equal to zero, and enforcing the symmetry condition of zero gradient for all the other variables by fitting a quadratic polynomial through the first three grid points, that is,

$$Q^i_{j,i} = \frac{4Q^i_{j,2} - Q^i_{j,3}}{3}$$

Problems encountered when this relationship was not used have also been discussed in reference 15.

The initial conditions at the data plane representing the jet exit $x = 0$ were chosen in a very rudimentary manner (except in the one case described in the section "Results and Discussion" under the heading "Smooth Initial Profile"). Since too many points would be necessary to describe the actual merging of the free-stream and duct flows just past a jet exit, the initial jet and free-stream u-velocity profiles were represented by two distinct flows, separated by a sharp boundary. Computationally, this relationship yields a one grid-point discontinuity between u_{jet} and u_∞. This initial condition is probably the most severe that can be imposed while still generating an eventually realistic flow description. For simplicity, the initial values of the crossflow velocities in the plane $x = 0$ were set equal to zero.

The pressure distribution was chosen to be uniform at the free-stream level since an unmatched static pressure would undoubtedly produce shocks. These shocks were not consciously sought as part of the problem, and the initial conditions were set to try to avoid their generation. The streamwise velocity and temperature levels were computed by assuming constant total temperature in the jet and free stream and specifying the jet and free-stream Mach numbers.

Solution of Matrix Equation

By using the extrapolation (eq. (22)) for the nonlinear coefficients and cross derivatives in equations (16) to (20), the ADI difference approximation for these equations results in a linear set of five equations in five unknowns at each step of the ADI marching procedure. Rather than make the quite arbitrary choice of the order of solution if a sequential technique of solving each equation in turn were elected, the five equations are coupled and solved simultaneously. The procedure is quite advantageous because, in addition to eliminating the choice of solution order, it models the physics more precisely by allowing changes in any variable to be instantaneously sensed by all the others. The resulting

matrix equation for the sweep of the ADI procedure where the z-derivatives are differenced implicitly has a block tridiagonal structure, one line of which can be represented as

$$\left[A_k\right]\vec{W}_{k+1} + \left[B_k\right]\vec{W}_k + \left[C_k\right]\vec{W}_{k-1} = \vec{D}_j \tag{23}$$

where the unknown vector $\vec{W}_k$ contains the five unknowns

$$\vec{W}_k = (u,v,w,T,p)^T \tag{24a}$$

the coefficients $\left[A\right]$, $\left[B\right]$, and $\left[C\right]$ are matrices, for example,

$$\left[A\right] = \begin{bmatrix} a_{11} & a_{12} & \cdot & \cdot & \cdot & a_{15} \\ a_{21} & a_{22} & \cdot & \cdot & \cdot & a_{25} \\ \cdot & \cdot & & & & \cdot \\ \cdot & \cdot & & & & \cdot \\ \cdot & \cdot & & & & \cdot \\ a_{51} & a_{52} & \cdot & \cdot & \cdot & a_{55} \end{bmatrix} \tag{24b}$$

and the vector $\vec{D}$ is the source term in each equation. The components a_{mn} represent the coefficient of the nth unknown from the mth equation at point k and are given in appendix B. The inversion of this block matrix is a standard procedure. (See ref. 21.)

Computer Requirements

The equations describing the flow were solved in the transformed plane $0 \leqq \eta, \zeta \leqq 1$. A uniform grid spacing in η and in ζ was used to insure second-order accuracy. Two different meshes were used for all the computations, a coarse grid of 21×21 points and a finer grid of 41×41 points. The core storage required for each of these programs was $60K_8$ and $151K_8$, respectively. The time required at each x station to process one unknown at one (η,ζ) point was approximately 0.00165 second per unknown per point on a CDC 6600 computer. This time is slower than the value of 0.0005 for a sequential ADI scheme used on a time asymptotic Navier-Stokes solution (ref. 23), but compares very well with the approximate value of 0.0313 computed from the 30 seconds of CDC 7600 computer time, quoted in reference 10, for a 50×23 grid (assuming a CDC 7600 computer is 6 times faster than a CDC 6600 computer). Thus, to compute one x-step of the PENS

procedure took 3.6 seconds for the 21×21 grid and 13.9 seconds for the 41×41 grid. Typical runs consisted of approximately 100 steps.

RESULTS AND DISCUSSION

The supersonic jet flow problem was solved for a number of different free-stream, geometrical, and computational conditions; these are summarized in table I. In all cases, (1) the Prandtl number N_{Pr} was set equal to unity, (2) the reference length was set equal to the minimum initial orifice width of the 1×1 square jet, (3) the pressure distribution was taken to be uniform at the free-stream value throughout the domain at $x = 0$, (4) the initial velocity distribution was discontinuous except in the case labeled hyperbolic tangent profile in table I, (5) the total temperature in the entire field was set equal to a constant at $x = 0$, and (6) the ratio of initial jet to free-stream Mach numbers was always 1.5.

The marching procedure followed for all runs was to initially use a step size Δx which was small compared with the core length of the jet being calculated, and then increment the x-step size occasionally in the march in order to be able to reach significant downstream distances from the jet orifice.

The main purpose of the test cases was to demonstrate the applicability of the equations, numerical procedure, and computer code. For axisymmetric or two-dimensional flow, the usual boundary-layer assumptions hold, and a standard free shear layer computation can be used to generate the flow. These two limiting geometric cases (two-dimensional and axisymmetric) are used as references for all the three-dimensional calculations. A square jet and increasing aspect ratio rectangular jets were computed. The square jet will be seen to behave much like an axisymmetric jet and the rectangular jets reproduce two-dimensional behavior for a part of the distance away from the orifice, but ultimately all the jets resemble axisymmetric ones at large distances downstream. A circular jet was also approximated in the three-dimensional Cartesian grid, and the differences between this and the previously computed flows are noted in addition to a comparison with the free shear layer calculation. A final case of interacting jets is shown to demonstrate the range of problems which can be handled.

Thus, in each case (except the interacting jets) a comparison will be made between the PENS results and the results obtained by using a classical shear layer jet (SLJ) code (ref. 24) of high accuracy.

In all the cases to be presented since $N_{Pr} = 1$ and the initial total temperature was constant, it was expected that this constancy would remain throughout the calculation. During the initial stages of jet development, there was about a 5-percent deviation from this constant, but when the calculation began to approximate the true asymptotic boundary-layer behavior, described in the subsequent sections, the constant total temperature relation was well approximated.

Square and Axisymmetric Jets

The variation of the velocity on the center line of the computed $M_j = 1.8$, $N_{Re} = 10$ jet with distance downstream of the initial orifice location is shown in figure 2. This gross feature of the flow is an excellent indicator of both the qualitative and quantitative aspects of the calculation method. On the low storage 21×21 grid, two transformations corresponding to different values of the constant A and B in equation (15) were used. The relation between points in the physical and computational plane is shown in table II. Thus for $A = B = \frac{1}{2}$, only 5 points are originally in the jet at $x = 0$ compared with 11 points in the jet when $A = B = 2$. The center-line velocity is noticeably affected as seen in figure 2, with the $A = B = 2$ case being shifted toward the shear layer result. An important detail which cannot be seen on the scale plotted in figure 2(a) is an overshoot of the center-line velocity in all cases when $A = B = \frac{1}{2}$ was used with this grid. Although the amount of overshoot was not particularly high (0.3 percent), it did indicate the presence of an inaccuracy. When the constant in the transformation was changed to $A = B = 2$, a monotonic decay of the center-line velocity always occurred.

For even greater accuracy, a 41×41 grid was used for the square jet, along with a transformation of $A = B = 2$. Again, a noticeable shift in the center-line decay curve toward the axisymmetric value is apparent. In an attempt to reproduce the SLJ code results used as a comparison in all these cases, a pseudo-circular geometry was constructed on the 41×41 grid. The resulting "circle" is shown in figure 3. The difference in area of the "circle" from a true circle is about 1 percent. The resulting center-line decay was indeed close to the SLJ value. (See fig. 2.)

One reason for the discrepancy of the approximate circle from the SLJ case and, in fact, a reason for the continual approach of the four curves (21×21, $A = B = \frac{1}{2}$; 21×21, $A = B = 2$; 41×41, $A = B = 2$; "circle") to the SLJ case is the difference in initial momenta (or for these cases, area) of each jet at $x = 0$. Since a discontinuous profile was assumed for the initial velocities, there is an additional amount of momentum contained between the last grid point at the jet edge, and the next grid point which is in the free stream. This additional momentum delays the velocity decay somewhat, as seen by the displacement of the curves in figures 2(a) and 2(b). As the grid size is decreased either by adjusting the transformation constants or by increasing the number of nodes, the initial momentum contained within the one grid step beyond the edge of the jet decreases and gives the results shown. The significant difference between the square and approximate circle curves is caused by the 22-percent reduction in area from a square to its inscribed circle. However, there is again an incremental area difference between the approximate circle and the axisymmetric case used for comparison. Since the SLJ code had 256 grid points, its approximation to a circle was very good. On the other hand, the PENS code had about 8 percent more momentum beyond the jet than was contained in it. This could certainly account for the shift of the PENS curve away from the SLJ curve.

As a final check on the ability of the code to compute correctly, at least for global features of the flow such as center-line decay, a comparison was made at $M_j = 1.8$ of square jets with Reynolds numbers of 10 and 1000. This comparison is shown in figure 4. The curves are identical to the scale used for the plotting; table III presents the computed values, and the difference is seen to be usually in the third significant figure. Hence the computation reproduces the correct Reynolds number scaling for an axisymmetric jet. (See ref. 2.)

A more severe test of the accuracy of the computer code is a comparison of actual velocity profiles rather than an integrated feature of the flow, such as the center-line decay rate. Figure 5 shows a comparison of the u velocity profile calculated for a circular jet with a Reynolds number of 10 and a jet Mach number of 1.8. Since it has already been seen that the PENS deck initially carries more momentum and will not exactly reproduce the x-wise behavior of the SLJ deck, two x-positions corresponding to approximately the same center-line velocity were compared. The results of the SLJ curve are for $\frac{x}{h} = 2.3$, whereas the $\frac{x}{h} = 2.5$ points are plotted for the PENS curve. Since these x-positions are in the asymptotic similarity region of the jet, equal center-line velocities should produce comparable profiles; figure 5 verifies this assertion. The two profiles almost coincide. It should also be noted that all the y-points used in the PENS calculation which fit within the scale of the plot are shown, but for the highly accurate SLJ calculation 175 points were within the plotting scale; thus only a few are shown.

The most sensitive of all the computed variables is the velocity component normal to the free stream in the cross planes. In the PENS calculation where the pressure gradients in the cross planes are actually computed and act as a driving force for v and w, these crossflows are highly influenced by any irregularities in the flow field. This is an important feature of the parabolic-elliptic Navier-Stokes calculation procedure and points out a significant difference between this method and standard shear layer calculations. The boundary-layer assumptions give the imposed pressure through the shear layer from the reduced normal momentum equation. The normal velocity is then computed from the continuity equation used in an auxiliary role to conserve mass. In the PENS procedure the momentum equations are used to compute the velocities and continuity gives the pressure. The roles of the equations and the variables they generate are completely reversed in the two techniques; see reference 25 for a further discussion.

The computed crossflows for the $N_{Re} = 10$, $M_j = 1.8$ circular jet are shown in figure 6. Here the agreement between PENS and SLJ is still good in the major portion of the jet, but deteriorates in the outer region. Also, there are obvious ripples in the PENS solution. This behavior is caused by oscillations in the computed pressure around the initial orifice location, $\frac{y}{h} = \frac{1}{2}$, and can be traced back to the initial discontinuity in the velocity and temperature profiles. An initial fluctuation in the pressure develops

(ref. 13) but eventually decays so that pressure in the cross plane is effectively a constant (the free-stream value). However, superimposed on this constant value are oscillations which are essentially undamped. (See appendix A.) Since the cross velocities are small $(\approx 10^{-3})$, relatively small oscillations in the pressure will be felt through the pressure gradient terms in the cross momentum equations. However, the results are quite good despite the oscillations present. (See fig. 6.)

The effect of the pressure terms can be seen more clearly if a comparison of velocity profiles is made further upstream in the jet flow near the end of the core region. Figure 7 shows the u-velocity for both PENS and SLJ calculations at $x = 0.13$ when the center-line velocity ratio $(u_{\text{℄}} - U_\infty)/(u_{\text{℄}} - U_\infty)_{x=0}$ is still equal to one. Again, the two curves are almost coincident. However, the comparison of v is striking. (See fig. 8.) The SLJ calculation shows the typical jet crossflow profile. The PENS result is very different. Here the v-profile almost precisely follows the cross-plane pressure gradient set up by the discontinuous initial profiles. Obviously, the pressure and cross-velocity effects combine to give the correct behavior of the main flow as evidenced by the agreement in figures 5 and 7 and the eventual agreement of the cross velocity further downstream (fig. 6). This demonstrates that the PENS and SLJ procedures react differently to the initial profiles. In the SLJ code all discrepancies of the flow are absorbed by the normal velocity through the continuity equation. The PENS code has an additional degree of freedom (the calculation of the pressure) and so initially adjusts differently, but eventually computes a standard shear layer flow.

Additional calculations were made for $M_j = 1.8$, $N_{Re} = 1000$, and $M_j = 7.5$, $N_{Re} = 1000$. The center-line velocity decay for the $M_j = 1.8$, $N_{Re} = 1000$ jet is shown in figure 9. The 41×41 square jet has already been compared for a Reynolds number scaling with the $N_{Re} = 10$ jet in figure 4. The center-line velocity plot for the $M_j = 7.5$, $N_{Re} = 1000$ case is shown in figure 10, the results being similar to the others thus far presented. A comparison of the PENS and SLJ u-velocity profiles is given in figure 11 for the $M_j = 1.8$, $N_{Re} = 1000$ circular case. Again, these comparisons show good agreement between PENS and SLJ calculations. However, no comparisons can be made of the cross velocity due to the behavior of the calculated pressure. Whereas the $N_{Re} = 10$ jet exhibited oscillations only in the YZ plane, for the $N_{Re} = 1000$ cases, an oscillation also appears in X. It is small (usually third or fourth decimal place) but significant. On alternate x-steps the pressure oscillates about the free-stream value of 1, and causes the y- and z-pressure gradients to change; hence, v and w change sign at successive x-steps and give nonphysical results. It is concluded that at this higher Reynolds number, the initial discontinuity affects the solution severely, much more than it did in the $N_{Re} = 10$ case.

Smooth Initial Profile

To test the solution procedure for less drastic initial profiles than the discontinuous ones used previously, a smooth, hyperbolic tangent initial profile was used for u in the PENS code. Again, the total temperature was assumed to be constant at $x = 0$, and the other variables were initialized as before. The initial u profile had no core region near the axis and so diffused rapidly once the PENS marching procedure was initiated.

The center-line decay rate is shown in figure 12 for the $N_{Re} = 10$, $M_j = 1.8$ PENS approximate-circular and axisymmetric SLJ cases. The agreement is very good. The u-velocity profiles compare very well with each other over the entire x-range computed. The normal velocity components behave in the same way as before, except that there are no oscillations in the solution, unlike those shown previously.

Even more important than the elimination of the low Reynolds number oscillations, the smooth initial profile allows the calculation of sensible crossflows at the higher Reynolds number of 1000. (See fig. 13 for a comparison of PENS and SLJ calculations.) Using the previous discontinuous profile produced meaningless values of v and w because of ripples in the calculated pressure. These ripples, although not completely eliminated, are reduced by more than three orders of magnitude when the smooth initial data were used, and their effect on the crossflow is greatly diminished.

Varying Aspect Ratio Rectangular Jets

The three-dimensional capability of the PENS code can be tested by varying the aspect ratio of the initial profiles, from the square one used previously, to rectangular profiles of large width-height ratios. These high-aspect-ratio jets should reproduce two-dimensional behavior near the center line for some distance downstream of the initial station until the effect of the initial edge of the jet propagates in far enough to change the flow to a three-dimensional one.

An excellent way to display this phenomenon is, again, to plot the streamwise velocity on the center line. Figure 14 shows, for $N_{Re} = 10$, $M_j = 1.8$ jets, the center-line velocity decay. A 4×1 rectangular jet and an 8×1 jet are displayed, along with a shear layer calculation of true two-dimensional jet. The two rectangular jets closely follow the SLJ results far downstream before three-dimensional effects alter the decay curve and finally cause it to decay in an axisymmetric manner. Initially, the two rectangular jets follow exactly the same curve. Beyond some location $\left(\text{approximately } \frac{x}{h} = 3 \text{ in fig. 14}\right)$, the outer edge of the initial profile is sensed earlier in the 4×1 case than in the 8×1 case, and the center line accordingly decays more rapidly. In the final stage of their decay, both jets behave axisymmetrically. In fact, they very nearly simulate the expected behavior with regard to their initial momenta. Since the static temperature at this stage

is very nearly equal to the free-stream value throughout the jet, the incompressible decay rate for axisymmetric jets,

$$\frac{u_{\mathfrak{L}}}{U_\infty} = \frac{3}{8\pi} \frac{KN_{Re}}{x/h}$$

(see ref. 2, eq. (10.19)) where K is the nondimensional initial jet momentum, can be used as a comparison. This relation shows that for equal ratios of initial momenta to x/h, the center-line velocity should be the same. Since the momentum in the 8×1 jet is twice that of the 4×1 jet, the velocity of the 8×1 jet should be equal to that of the 4×1 jet at half the x/h of the 8×1 jet. The values shown in figure 14 very nearly confirm this ratio.

One further point about the results of figure 14 should be noted. The computed two-dimensional decay rate is not the usual value of $x^{-1/3}$ of two-dimensional incompressible flows. (See ref. 2.) This was noted previously by Pai (ref. 26) who attributed it to the presence of heat transfer.

The u- and v-velocity profiles computed by the PENS method for an 8×1 rectangle (at $x/h = 1.5$) and the SLJ method (at $x/h = 1.3$) are shown in figures 15 and 16. The different x-locations were chosen to equate the center-line velocities as previously described. Close to the axis, both calculations agree very well, but in the outer region of the jet, there is a substantial difference. The PENS jet has spread further into the free stream.

As these x-locations are not in the asymptotic decay region, exact comparisons should not be expected and the excess spread of the PENS jet, calculated from a true three-dimensional procedure, can be explained. To reach the given value of center-line velocity shown, the PENS calculation has to proceed further downstream and hence will spread somewhat more than the SLJ jet.

The true three-dimensional nature of the PENS calculation also contributes to the additional spread by removing the constraint of only one direction from which entrained momentum may be drawn. The effect of the second cross stream direction is always felt, although initially it is small, and allows another degree of freedom by which the jet may spread.

For the higher Reynolds number jets, the same quantitative behavior was obtained in the rectangular cases as in the square and circular cases.

Interacting Jets

As an example of the wider range of geometries which can be handled by the PENS calculation method, a case of the flow generated by two interacting jets was computed.

Two square jets of width h, separated by a distance h, were computed under the same flow conditions as previously used in some of the PENS test cases, that is, $M_\infty = 5.0$, $M_j = 7.5$, $N_{Re} = 1000$. (See table I.)

This sort of geometrical configuration is of interest in the aerodynamic integration of exhaust nozzles on the current F-15 configuration into the fuselage. This integration entails the present configuration containing two axisymmetric nozzles altered as shown in figure 17 to contain two two-dimensional (rectangular) nozzles. No attempt was made in the calculation to duplicate the actual conditions of an F-15 nozzle; one of the cases calculated previously was simply run with altered initial geometry to simulate the interacting jets. No difficulties were encountered with this computation.

Figure 18 shows the behavior of the streamwise velocity on the symmetry line between the two jet exits, the square and 4×1 rectangular jet results being included for reference. Initially, on the center line the velocity is the free-stream value and initially increases as the influence of the jet is felt. Eventually though, the offset jets merge and the center-line velocity starts to level off and then decay quickly, axisymmetric behavior being assumed. Figure 19 shows the computed streamwise velocity profiles on the symmetry line, and figure 20 shows these computed velocities in a perspective plot for the half plane $y \geq 0$ of the flow domain. These results are qualitatively correct; however, no comparisons can be made with shear layer calculations since this three-dimensional flow is beyond the scope of boundary-layer theory.

Possibility of Extending the PENS Method to Turbulent Flows

All the comparisons of PENS and SLJ calculations which have been made thus far have been for laminar flows. It will now be necessary to include the appropriate turbulence model for these flows in order to extend the applicability of the procedure. A second-order turbulence closure method has already been used with the incompressible PENS approximation in the calculation of submarine wakes without reported difficulty. (See ref. 12.) Hence, in principle, a compressible model should pose no insurmountable problems, although the task is by no means simple. In fact, the inclusion of turbulence modeling into the solution procedure may very well take better advantage of the present PENS procedure since the coupled solution technique is almost certainly necessary in the turbulent case (ref. 27), but is probably not essential for the solution of the laminar flow. Although the models complicate the governing equations, perhaps making them more difficult to solve, the effective Reynolds number of the flow is reduced by the addition of turbulence; and the lower Reynolds number cases which have been computed yielded significantly smoother results.

CONCLUDING REMARKS

In all cases where comparisons could be made with shear layer calculations, the parabolic-elliptic Navier-Stokes calculations produced results which compared well, not only with gross characteristics of the flow, such as center-line decay rate, but also with detailed profile calculations, except in the initial stages of the flow development where the procedure calculates a pressure gradient across the shear layer, to which the crossflow velocity reacts differently than a standard shear layer flow.

The alternating direction implicit method has been successfully applied in a numerical solution of these PENS equations. A coordinate transformation was introduced which allowed the imposition of free-stream (that is, infinity) boundary conditions at a finite location in the computational domain. This transformation eliminated any difficulties caused by an arbitrary choice of free-stream location in the untransformed plane but created some difficulties of its own. Too large a coordinate stretching in a region of significant flow proved to yield inaccurate and nonphysical results.

Discontinuous initial conditions were used and produced smooth results at low Reynolds numbers, but in the higher Reynolds number cases oscillations in the pressure caused a deterioration of the calculated crossflow. This problem was alleviated by using a smooth initial profile. Thus, if experimental data were used at the initial station, it is assumed that no difficulties would ensue, since the data would presumably be smooth.

Computed results have been presented for various jet configurations. Although the character of the computed flow can be predominantly axisymmetric in the case of the square jet or approach a two-dimensional limit as is the case for the 8×1 rectangular jet, no prior assumptions to this effect are required. The solution computes the particular flow under investigation as though it were three-dimensional and allows the initial geometry of the prescribed jet to determine the ultimate nature of the solution.

A final configuration studied consisted of two square jets symmetrically disposed about a symmetry axis. This is a simple geometric model of the exhaust of a proposed F-15 modification and demonstrates the range of geometries which can be handled.

The parabolic-elliptic Navier-Stokes equations have been shown to model adequately flows where the two crossflow directions are of equal importance in a predominantly convective viscous flow.

Langley Research Center
National Aeronautics and Space Administration
Hampton, VA 23665
August 12, 1976

APPENDIX A

STABILITY AND DAMPING OF THE ADI METHOD

Any of the governing equations used to solve the jet problem (eqs. (16) to (20)) can be linearized to give the simple form

$$\frac{\partial Q}{\partial x} + a\frac{\partial Q}{\partial y} + b\frac{\partial Q}{\partial z} = \alpha\left(\frac{\partial^2 Q}{\partial y^2} + \frac{\partial^2 Q}{\partial z^2}\right) \tag{A1}$$

Note that the following analysis is only for one equation in one unknown, and not for the entire coupled system (eqs. (16) to (20)) for which the analysis is much more difficult. However, as each equation can be thought of as influencing one particular variable more than any other, that is, momentum equations and corresponding velocities, energy equation and T, and continuity equation and p, some insight into the numerical behavior of the ADI method can be obtained.

By using the ADI method, the difference form of equation (A1) becomes

$$\frac{Q^*_{l,m} - Q^n_{l,m}}{(\Delta x/2)} + a\delta_y Q^n_{l,m} + b\delta_z Q^*_{l,m} = \alpha\left(\delta_y^2 Q^n_{l,m} + \delta_z^2 Q^*_{l,m}\right) \tag{A2}$$

$$\frac{Q^{n+1}_{l,m} - Q^*_{l,m}}{(\Delta x/2)} + a\delta_y Q^{n+1}_{l,m} + b\delta_z Q^*_{l,m} = \alpha\left(\delta_y^2 Q^{n+1}_{l,m} + \delta_z^2 Q^*_{l,m}\right) \tag{A3}$$

where l and m are the discretized y- and z-positions and *, n, and n+1 are the discretized x-positions. Performing a Von Neumann stability analysis using

$$Q^n_{l,m} = Q^n e^{i\left(lk_y\Delta y + mk_z\Delta z\right)}$$

in equations (A2) and (A3) gives

$$Q^* - Q^n + ic_y Q^n \sin\phi_y + ic_z Q^* \sin\phi_z = \beta_y Q^n\left(\cos\phi_y - 1\right) + \beta_z Q^*\left(\cos\phi_z - 1\right)$$

$$Q^{n+1} - Q^* + ic_y Q^{n+1} \sin\phi_y + ic_z Q^* \sin\phi_z = \beta_y Q^{n+1}\left(\cos\phi_y - 1\right) + \beta_z Q^*\left(\cos\phi_z - 1\right)$$

where

$$c_y = \frac{a\Delta x}{2\Delta y}$$

$$\beta_y = \frac{\alpha \Delta x}{\Delta y^2}$$

$$\phi_y = k_y \Delta y$$

and

$$c_z = \frac{a\Delta x}{2\Delta z}$$

$$\beta_z = \frac{\alpha \Delta x}{\Delta z^2}$$

$$\phi_z = k_z \Delta z$$

Therefore,

$$G^* = \frac{Q^*}{Q^n} = \frac{1 - ic_y \sin \phi_y - \beta_y(1 - \cos \phi_y)}{1 + ic_z \sin \phi_z + \beta_z(1 - \cos \phi_z)}$$

$$G^{n+1} = \frac{Q^{n+1}}{Q^*} = \frac{1 - ic_z \sin \phi_z - \beta_z(1 - \cos \phi_z)}{1 + ic_y \sin \phi_y + \beta_y(1 - \cos \phi_y)}$$

and therefore the amplification factor G for the complete step is

$$G = G^* G^{n+1} = \frac{1 - ic_y \sin \phi_y - \beta_y(1 - \cos \phi_y)}{1 + ic_y \sin \phi_y + \beta_y(1 - \cos \phi_y)} \frac{1 - ic_z \sin \phi_z - \beta_z(1 - \cos \phi_z)}{1 + ic_z \sin \phi_z + \beta_z(1 - \cos \phi_z)} \tag{A4}$$

Hence $|G| \leq 1$ and the method is stable for the convection-diffusion equation (A1).

If equation (A1) is simplified so that there are only convective terms, that is, $\alpha = 0$, then it becomes a simple linearized model of the continuity equation (where $Q = p$). For this case, the amplification factor (eq. (A4)) becomes

$$G = \frac{1 - ic_y \sin \phi_y}{1 + ic_y \sin \phi_y} \frac{1 - ic_z \sin \phi_z}{1 + ic_z \sin \phi_z}$$

The magnitude of G is therefore

$$|G| = 1$$

exactly, and the numerical scheme introduces no damping. Oscillations which may occur in the solution do not decay and persist undamped (unless affected by a coupling to the other equations where viscous terms are present). This is not the case for any other implicit scheme except a Crank-Nicolson differencing, which is equivalent to the ADI method within the second-order truncation error. (See ref. 28.)

A general implicit scheme (ref. 28) for equation (A1) with $\alpha = 0$ gives for the amplification factor

$$G = \frac{1 - i(1 - \theta)\left(c_y \sin \phi_y + c_z \sin \phi_z\right)}{1 + i\theta\left(c_y \sin \phi_y + c_z \sin \phi_z\right)}$$

where $\theta = \frac{1}{2}$ gives Crank-Nicolson differencing and $\theta = 1$ gives a fully implicit differencing. The magnitude of G is

$$|G| = \frac{1 + (1 - \theta)^2\left(c_y \sin \phi_y + c_z \sin \phi_z\right)^2}{1 + \theta^2\left(c_y \sin \phi_y + c_z \sin \phi_z\right)^2} \tag{A5}$$

To find the damping, look at the long wavelength disturbances by letting ϕ_y and ϕ_z approach zero simultaneously, and expand the denominator of equation (A5) to get

$$|G| = \left[1 + (1 - \theta)^2\left(c_y\phi_y + c_z\phi_z\right)^2\right]\left[1 - \theta^2\left(c_y\phi_y + c_z\phi_z\right)^2 + \ldots\right]$$

Thus

$$|G| = 1 + (1 - 2\theta)\left(c_y\phi_y + c_z\phi_z\right)^2 + \ldots$$

and for only $\theta = \frac{1}{2}$, that is, Crank-Nicolson differencing, is the amplification factor identically equal to unity. For $\theta = 1$, a fully implicit scheme, significant second-order damping occurs.

APPENDIX B

MATRIX COEFFICIENTS OF THE LINEARIZED DIFFERENCE EQUATIONS

In equation (23), for the first half of the ADI procedure, from a location i to the intermediate * location, the components of the matrices [A], [B], [C], and the vector $\vec{D}$ are

$$a_{11} = \frac{1}{2}\left[\rho w + 2B(1-\zeta)\mu/N_{Re}\right]B(1-\zeta)^2/\Delta\zeta - B^2(1-\zeta)^4\left[\mu/\Delta\zeta^2 + \frac{1}{4}\frac{\partial\mu}{\partial T}\frac{\partial T}{\partial\zeta}\Big/\frac{1}{\Delta\zeta}\right]\Big/N_{Re}$$

$$a_{12} = 0$$

$$a_{13} = 0$$

$$a_{14} = -\left[\frac{1}{4}B^2(1-\zeta)^4\frac{\partial\mu}{\partial T}\frac{\partial u}{\partial\zeta}/N_{Re}\right]\Big/\Delta\zeta$$

$$a_{15} = 0$$

$$a_{21} = 0$$

$$a_{22} = a_{11}$$

$$a_{23} = \left[\frac{1}{6}AB(1-\eta)^2(1-\zeta)^2\frac{\partial\mu}{\partial T}\frac{\partial T}{\partial\eta}/N_{Re}\right]\Big/\Delta\zeta$$

$$a_{24} = -\left\{\frac{1}{4}\left[B^2(1-\zeta)^4\frac{\partial v}{\partial\zeta} + AB(1-\zeta)^2(1-\eta)^2\frac{\partial w}{\partial\eta}\right]\frac{\partial\mu}{\partial T}/N_{Re}\right\}\Big/\Delta\zeta$$

$$a_{25} = 0$$

$$a_{31} = 0$$

$$a_{32} = -\left[\frac{1}{4}AB(1-\eta)^2(1-\zeta)^2\frac{\partial\mu}{\partial T}\frac{\partial T}{\partial\eta}/N_{Re}\right]\Big/\Delta\zeta$$

$$a_{33} = \frac{1}{2}\left[\rho w + \frac{8}{3}B(1-\zeta)\mu/N_{Re}\right]B(1-\zeta)^2/\Delta\zeta - \frac{1}{3}B^2(1-\zeta)^4\left[4\mu/\Delta\zeta^2 + \frac{\partial\mu}{\partial T}\frac{\partial T}{\partial\zeta}/\Delta\zeta\right]\Big/N_{Re}$$

$$a_{34} = \left\{\frac{1}{3}\left[\frac{1}{2}AB(1-\eta)^2(1-\zeta)^2\frac{\partial v}{\partial\eta} - B^2(1-\zeta)^4\frac{\partial w}{\partial\zeta}\right]\frac{\partial\mu}{\partial T}/N_{Re}\right\}\Big/\Delta\zeta$$

$$a_{35} = \left[\frac{1}{2}B(1-\zeta)^2/\left(\gamma M_\infty^2\right)\right]\Big/\Delta\zeta$$

APPENDIX B

$$a_{41} = -\left[E_\infty \mu B^2 (1-\zeta)^4 \frac{\partial \mu}{\partial \zeta} \Big/ N_{Re}\right] \Big/ \Delta\zeta$$

$$a_{42} = -\left\{\frac{1}{2} E_\infty \mu \left[B^2 (1-\zeta)^4 \frac{\partial v}{\partial \zeta} + AB(1-\eta)^2 (1-\zeta)^2 \frac{\partial w}{\partial \eta}\right] \Big/ N_{Re}\right\} \Big/ \Delta\zeta$$

$$a_{43} = -\left\{\frac{2}{3} E_\infty \mu \left[B^2 (1-\zeta)^4 \partial w - \frac{1}{2} AB(1-\eta)^2 (1-\zeta)^2 \frac{\partial v}{\partial \eta}\right] \Big/ N_{Re}\right\} \Big/ \Delta\zeta$$

$$a_{44} = \left\{\frac{1}{2}\left[\rho w + 2B(1-\zeta)\mu / N_{Re} / N_{Pr}\right] B(1-\zeta)^2 / \Delta\zeta - B^2 (1-\zeta)^4 \left[\mu / \Delta\zeta^2 + \frac{1}{2} \frac{\partial \mu}{\partial T} \frac{\partial T}{\partial \zeta} / \Delta\zeta\right] \Big/ N_{Re}\right\} \Big/ N_{Pr}$$

$$a_{45} = -\frac{1}{2} \frac{(\gamma - 1)}{\gamma} B(1-\zeta)^2 w / \Delta\zeta$$

$$a_{51} = 0$$

$$a_{52} = 0$$

$$a_{53} = \frac{1}{2} B(1-\zeta)^2 p / \Delta\zeta$$

$$a_{54} = -\frac{1}{2} B(1-\zeta)^2 \rho w / \Delta\zeta$$

$$a_{55} = \frac{1}{2} B(1-\zeta)^2 w / \Delta\zeta$$

$$b_{11} = 2\rho u / \Delta\xi_+ + \left[2B^2 (1-\zeta)^4 \mu / N_{Re}\right] / \Delta\zeta^2$$

$$b_{12} = 0$$

$$b_{13} = 0$$

$$b_{14} = 0$$

$$b_{15} = \left(2 / \Delta\xi_+\right) / \gamma M_\infty^2$$

$$b_{21} = 0$$

$$b_{22} = b_{11}$$

$$b_{23} = 0$$

$$b_{24} = 0$$

$$b_{25} = 0$$

APPENDIX B

$$b_{31} = 0$$

$$b_{32} = 0$$

$$b_{33} = 2\rho u/\Delta\xi_+ + \left[\frac{8}{3} B^2(1 - \zeta)^4 \mu/N_{Re}\right]/\Delta\zeta^2$$

$$b_{34} = 0$$

$$b_{35} = 0$$

$$b_{41} = 0$$

$$b_{42} = 0$$

$$b_{43} = 0$$

$$b_{44} = 2\rho u/\Delta\xi_+ + \left\{\left[2B^2(1 - \zeta)^4 \mu/N_{Re}\right]/N_{Pr}\right\}/\Delta\zeta^2$$

$$b_{45} = -2\frac{(\gamma - 1)}{\gamma} u/\Delta\xi_+$$

$$b_{51} = 2p/\Delta\xi_+$$

$$b_{52} = 0$$

$$b_{53} = 0$$

$$b_{54} = -2\rho u/\Delta\xi_+$$

$$b_{55} = 2u/\Delta\xi_+$$

$$c_{11} = -\frac{1}{2}\left[\rho w + 2B(1 - \zeta)\mu/N_{Re}\right]B(1 - \zeta)^2/\Delta\zeta - B(1 - \zeta)^4\left[\mu/\Delta\zeta^2 - \frac{1}{4}\frac{\partial\mu}{\partial T}\frac{\partial T}{\partial\zeta}/\Delta\zeta\right]/N_{Re}$$

$$c_{12} = 0$$

$$c_{13} = 0$$

$$c_{14} = -a_{14}$$

$$c_{15} = 0$$

APPENDIX B

$$c_{21} = 0$$

$$c_{22} = c_{11}$$

$$c_{23} = -a_{23}$$

$$c_{24} = -a_{24}$$

$$c_{25} = 0$$

$$c_{31} = 0$$

$$c_{32} = -a_{32}$$

$$c_{33} = -\frac{1}{2}\left[\rho w + \frac{8}{3} B(1 - \zeta)\mu / N_{Re}\right] B(1 - \zeta)^2 / \Delta\zeta - \frac{1}{3} B^2(1 - \zeta)^4 \left[4\mu / \Delta\zeta^2 - \frac{\partial\mu}{\partial T}\frac{\partial T}{\partial\zeta} / \Delta\zeta\right] / N_{Re}$$

$$c_{34} = -a_{34}$$

$$c_{35} = -a_{35}$$

$$c_{41} = -a_{41}$$

$$c_{42} = -a_{42}$$

$$c_{43} = -a_{43}$$

$$c_{44} = -\frac{1}{2}\left[\rho w + 2B(1 - \zeta)\mu / N_{Re} / N_{Pr}\right] B(1 - \zeta)^2 / \Delta\zeta - \left\{B^2(1 - \zeta)^4 \left[\mu / \Delta\zeta^2 - \frac{\partial\mu}{\partial T}\frac{\partial T}{\partial\zeta} / \Delta\zeta\right] / N_{Re}\right\} / N_{Pr}$$

$$c_{45} = -a_{45}$$

$$c_{51} = 0$$

$$c_{52} = 0$$

$$c_{53} = -a_{53}$$

$$c_{54} = -a_{54}$$

$$c_{55} = -a_{55}$$

APPENDIX B

$$d_1 = 2\rho u\, u^i_{j,k}/\Delta\xi_+ + \frac{2}{\gamma M_\infty^2}\, p^i_{j,k}/\Delta\xi_+ - \left[\rho v + 2A(1-\eta)\mu/N_{Re}\right] A(1-\eta)^2 \left.\frac{\partial u}{\partial \eta}\right|^i_{j,k}$$

$$+ A^2(1-\zeta)^4 \left[\mu \left.\frac{\partial^2 u}{\partial \eta^2}\right|^i_{j,k} + \frac{1}{2}\frac{\partial \mu}{\partial T}\left(\left.\frac{\partial T}{\partial \eta}\right|^i_{j,k} \left.\frac{\partial \mu}{\partial \eta}\right|^i_{j,k} + \left.\frac{\partial u}{\partial \eta}\right|^i_{j,k} \left.\frac{\partial T}{\partial \eta}\right|^i_{j,k} \right) \right] \Big/ N_{Re}$$

$$d_2 = 2\rho u\, v^i_{j,k}/\Delta\xi_+ - A(1-\eta)^2 \frac{1}{\gamma M_\infty^2} \left.\frac{\partial p}{\partial \eta}\right|^i_{j,k} - \left[\rho v + \frac{8}{3} A(1-\eta)\mu/N_{Re}\right] A(1-\eta)^2 \left.\frac{\partial v}{\partial \eta}\right|^i_{j,k}$$

$$+ A^2(1-\eta)^4 \left[\frac{4}{3}\mu \left.\frac{\partial^2 v}{\partial \eta^2}\right|^i_{j,k} + \frac{2}{3}\frac{\partial u}{\partial T}\left(\left.\frac{\partial T}{\partial \eta}\right|^i_{j,k} \left.\frac{\partial v}{\partial \eta}\right|^i_{j,k} + \left.\frac{\partial v}{\partial \eta}\right|^i_{j,k} \left.\frac{\partial T}{\partial \eta}\right|^i_{j,k} \right) \right] \Big/ N_{Re}$$

$$+ AB(1-\eta)^2(1-\zeta)^2 \left[\frac{1}{3}\mu \frac{\partial^2 w}{\partial \eta\, \partial \zeta} + \frac{\partial \mu}{\partial T}\left(\frac{1}{2}\left.\frac{\partial T}{\partial \zeta}\right|^i_{j,k} \left.\frac{\partial w}{\partial \eta}\right|^i_{j,k} - \frac{1}{3}\left.\frac{\partial w}{\partial \zeta}\right|^i_{j,k} \left.\frac{\partial T}{\partial \eta}\right|^i_{j,k} \right) \right] \Big/ N_{Re}$$

$$d_3 = 2\rho u\, w^i_{j,k}/\Delta\xi_+ - \left[\rho v + 2A(1-\eta)\mu/N_{Re}\right] A(1-\eta)^2 \left.\frac{\partial w}{\partial \eta}\right|^i_{j,k}$$

$$+ A^2(1-\eta)^4 \left[\mu \left.\frac{\partial^2 w}{\partial \eta^2}\right|^i_{j,k} + \frac{1}{2}\frac{\partial \mu}{\partial T}\left(\left.\frac{\partial T}{\partial \eta}\right|^i_{j,k} \left.\frac{\partial w}{\partial \eta}\right|^i_{j,k} + \left.\frac{\partial w}{\partial \eta}\right|^i_{j,k} \left.\frac{\partial T}{\partial \eta}\right|^i_{j,k} \right) \right] \Big/ N_{Re}$$

$$+ AB(1-\eta)^2(1-\zeta)^2 \left[\frac{1}{3}\mu \frac{\partial^2 v}{\partial \eta\, \partial \zeta} + \frac{\partial \mu}{\partial T}\left(\frac{1}{2}\left.\frac{\partial v}{\partial \zeta}\right|^i_{j,k} \left.\frac{\partial T}{\partial \eta}\right|^i_{j,k} - \frac{1}{3}\left.\frac{\partial T}{\partial \zeta}\right|^i_{j,k} \left.\frac{\partial v}{\partial \eta}\right|^i_{j,k} \right) \right] \Big/ N_{Re}$$

$$d_4 = 2\rho u\, T^i_{j,k}/\Delta\xi_+ - \left[\rho v + 2A(1-\zeta)\mu/N_{Re}/N_{Pr}\right] A(1-\eta)^2 \left.\frac{\partial T}{\partial \eta}\right|^i_{j,k}$$

$$+ \frac{(\gamma-1)}{\gamma}\left[A(1-\eta)^2 v \left.\frac{\partial p}{\partial \eta}\right|^i_{j,k} - 2up^i_{j,k}/\Delta\xi_+ \right] + A^2(1-\eta)^4 \left\{ \left[\mu \left.\frac{\partial^2 T}{\partial \eta^2}\right|^i_{j,k} \frac{\partial \mu}{\partial T}\left.\frac{\partial T}{\partial \eta}\right|^i_{j,k} \left.\frac{\partial T}{\partial \eta}\right|^i_{j,k} \right] \Big/ N_{Re} \right\} \Big/ N_{Pr}$$

$$+ E_\infty \mu \left[A^2(1-\eta)^4 \left(\left.\frac{\partial u}{\partial \eta}\right|^i_{j,k} \left.\frac{\partial u}{\partial \eta}\right|^i_{j,k} + \frac{4}{3}\left.\frac{\partial v}{\partial \eta}\right|^i_{j,k} \left.\frac{\partial v}{\partial \eta}\right|^i_{j,k} + \left.\frac{\partial w}{\partial \eta}\right|^i_{j,k} \left.\frac{\partial w}{\partial \eta}\right|^i_{j,k} \right) \right.$$

$$\left. + AB(1-\eta)^2(1-\zeta)^2 \left(\left.\frac{\partial v}{\partial \zeta}\right|^i_{j,k} \left.\frac{\partial w}{\partial \eta}\right|^i_{j,k} - \frac{2}{3}\left.\frac{\partial w}{\partial \zeta}\right|^i_{j,k} \left.\frac{\partial v}{\partial \eta}\right|^i_{j,k} \right) \right] \Big/ N_{Re}$$

$$d_5 = 2\left(up^i_{j,k} - \rho u\, T^i_{j,k} + pu^i_{j,k}\right)\Big/\Delta\xi_+ - A(1-\eta)^2\left[v\left.\frac{\partial p}{\partial \eta}\right|^i_{j,k} - \rho v\left.\frac{\partial T}{\partial \eta}\right|^i_{j,k} + p\left.\frac{\partial v}{\partial \eta}\right|^i_{j,k}\right]$$

where the unsubscripted field variables are evaluated at the point $\left(i + \frac{1}{2}, j, k\right)$ by the extrapolation (eq. (22)). The second half of the ADI step, from location $*$ to $i + 1$, has elements similar to these, but with the roles of η and ζ reversed.

REFERENCES

1. Free Turbulent Shear Flows. Volume I – Conference Proceedings. NASA SP-321, 1973.

2. Schlichting, Hermann (J. Kestin, transl.): Boundary Layer Theory. Fourth ed., McGraw-Hill Book Co., Inc., c.1960.

3. Rudman, S.; and Rubin, S. G.: Hypersonic Viscous Flow Over Slender Bodies With Sharp Leading Edges. AIAA J., vol. 6, no. 10, Oct. 1968, pp. 1883-1890.

4. Nardo, C. T.; and Cresci, R. J.: An Alternating Directional Implicit Scheme for Three-Dimensional Hypersonic Flows. J. Comput. Phys., vol. 8, no. 2, Oct. 1971, pp. 268-284.

5. Peaceman, D. W.; and Rachford, H. H., Jr.: The Numerical Solution of Parabolic and Elliptic Differential Equations. J. Soc. Ind. & Appl. Math., vol. 3, no. 1, Mar. 1955, pp. 28-41.

6. Rubin, S. G.; and Lin, T. C.: Numerical Methods for Two- and Three-Dimensional Viscous Flow Problems: Application to Hypersonic Leading Edge Equations. AFOSR-TR-71-0778, U.S. Air Force, Apr. 1971. (Available from DDC as AD 726 547.)

7. Rubin, Stanley G.; and Lin, Tony C.: A Numerical Method for Three-Dimensional Viscous Flow: Application to the Hypersonic Leading Edge. J. Comput. Phys., vol. 9, no. 2, Apr. 1972, pp. 339-364.

8. Lin, T. C.; and Rubin, S. G.: Viscous Flow Over a Cone at Moderate Incidence – I Hypersonic Tip Region. Computers & Fluids, vol. 1, no. 1, Jan. 1973, pp. 37-57.

9. Lubard, Stephen C.; and Helliwell, William S.: Calculation of the Flow on a Cone at High Angle of Attack. AIAA Paper No. 73-636, July 1973.

10. Helliwell, William S.; and Lubard, Stephen C.: An Implicit Method for Three Dimensional Viscous Flow With Application to Cones at Angle of Attack. Computers & Fluids, vol. 3, no. 1, Mar. 1975, pp. 83-101.

11. Patankar, S. V.; and Spalding, D. B.: A Calculation Procedure for Heat, Mass and Momentum Transfer in Three-Dimensional Parabolic Flows. Int. J. Heat and Mass Transfer, vol. 15, no. 10, Oct. 1972, pp. 1787-1806.

12. Lewellen, W. S.; Teske, M.; and Donaldson, Coleman duP.: Turbulent Wakes in a Stratified Fluid. Part I: Model Development, Verification, and Sensitivity to Initial Conditions. Rep. No. 226, Aeronaut. Res. Assoc. Princeton, Inc., Aug. 1972.

13. Hirsh, Richard S.: Calculation of Supersonic Three-Dimensional Free-Mixing Flows Using the Parabolic-Elliptic Navier-Stokes Equations. Aerodynamic Analyses Requiring Advanced Computers, Part I, NASA SP-347, 1975, pp. 543-565.

14. Pai, S. I.; and Hsieh, T. Y.: Linearized Theory of Three-Dimensional Jet Mixing With and Without Walls. Trans. ASME, ser. D: J. Basic Eng., vol. 92, no. 1, Mar. 1970, pp. 93-100.

15. Van de Vooren, A. I.; and Dijkstra, D.: The Navier-Stokes Solution for Laminar Flow Past a Semi-Infinite Flat Plate. J. Eng. Math., vol. 4, no. 4, Oct. 1970, pp. 9-27.

16. Davis, R. T.: Numerical Solution of the Navier-Stokes Equations for Symmetric Laminar Incompressible Flow Past a Parabola. J. Fluid Mech., vol. 51, pt. 3, Feb. 1972, pp. 417-433.

17. South, Jerry C., Jr.; and Jameson, Antony: Relaxation Solutions for Inviscid Axisymmetric Transonic Flow Over Blunt or Pointed Bodies. AIAA Computational Fluid Dynamics Conference, July 1973, pp. 8-17.

18. Roberts, Glyn O.: Computational Meshes for Boundary Layer Problems. Proceedings of the Second International Conference on Numerical Methods in Fluid Dynamics. Volume 8 of Lecture Notes in Physics, Maurice Holt, ed., Springer-Verlag, 1971, pp. 171-177.

19. Gough, D. O.; Spiegel, E. A.; and Toomre, Juri: Highly Stretched Meshes as Functionals of Solutions. Proceedings of the Fourth International Conference on Numerical Methods in Fluid Dynamics. Volume 35 of Lecture Notes in Physics, Richard D. Richtmyer, ed., Springer-Verlag, 1975, pp. 191-196.

20. Douglas, Jim, Jr.; and Jones, B. F., Jr.: On Predictor-Corrector Methods for Nonlinear Parabolic Differential Equations. J. Soc. Ind. & Appl. Math., vol. 11, no. 1, Mar. 1963, pp. 195-204.

21. Krause, E.; Hirschel, E. H.; and Bothmann, Th.: Differenzenformeln zur Berechnung Dreidimensionaler Grenzschichten (Finite Difference Equations for Calculating Three-Dimensional Boundary Layers). DLR FB 69-66, Sept. 1969.

22. Hixon, Barbara A.; Beckwith, Ivan E.; and Bushnell, Dennis M.: Computer Program for Compressible Laminar or Turbulent Nonsimilar Boundary Layers. NASA TM X-2140, 1971.

23. Rudy, David H.; Morris, Dana J.; Blanchard, Doris K.; Cooke, Charlie H.; and Rubin, Stanley G.: An Investigation of Several Numerical Procedures for Time-Asymptotic Compressible Navier-Stokes Solutions. Aerodynamic Analyses Requiring Advanced Computers, Part I, NASA SP-347, 1975, pp. 437-468.

24. Oh, Y. H.: Analysis of Two-Dimensional Free Turbulent Mixing. AIAA Paper No. 74-594, June 1974.

25. Lin, Tony C.: Hypersonic Viscous Interactions. Ph. D. Diss., Polytech. Inst. Brooklyn, June 1970.

26. Pai, Shih I.: Fluid Dynamics of Jets. D. Van Nostrand Co., Inc., c.1954.

27. Naot, D.; Shavit, A.; and Wolfshtein, M.: Numerical Calculation of Reynolds Stresses in a Square Duct With Secondary Flow. Wärme- und Stoffübertragung, vol. 7, no. 3, 1974, pp. 150-161.

28. Richtmyer, Robert D.; and Morton, K. W.: Difference Methods for Initial-Value Problems. Second ed., Interscience Publ., c.1967.

TABLE L - VARIOUS JET CONFIGURATIONS COMPUTED

Configuration	N_{Re} = 10; M_∞ = 1.2; M_j = 1.8	N_{Re} = 1000; M_∞ = 1.2; M_j = 1.8	N_{Re} = 1000; M_∞ = 5.0; M_j = 7.5
Square jet; 21 × 21 grid; A = B = $\frac{1}{2}$	✓		
Square jet; 21 × 21 grid; A = B = 2	✓	✓	✓
Square jet; 41 × 41 grid; A = B = 2	✓	✓	✓
4 × 1 rectangular jet; 41 × 41 grid; A = B = 2	✓	✓	
8 × 1 rectangular jet; 41 × 41 grid; A = 0.52; B = 2	✓		
Circular jet; 41 × 41 grid; A = B = 2	✓	✓	
Circular jet; 41 × 41 grid; hyperbolic tangent profile	✓	✓	
Interacting square jets; 41 × 41 grid; A = B = 2			✓

TABLE II.- EFFECT OF TRANSFORMATION CONSTANT ON LOCATION OF GRID POINTS IN THE PHYSICAL PLANE FOR A 21×21 GRID

η	$y\left(A = \frac{1}{2}\right)$	$y(A = 2)$
0.00	0.00	0.00
.05	.105	.026
.10	.222	.056
.15	.353	.088
.20	.500	.125
.25	.667	.167
.30	.857	.214
.35	1.077	.269
.40	1.333	.333
.45	1.636	.409
.50	2.000	.500
.55	2.444	.611
.60	3.000	.750
.65	3.714	.929
.70	4.667	1.167
.75	6.000	1.500
.80	8.000	2.000
.85	11.333	2.833
.90	18.000	4.500
.95	38.000	9.500
1.00	∞	∞

TABLE III.- CENTER-LINE VELOCITY RATIOS FOR $M_j = 1.8$ SQUARE JETS FOR TWO DIFFERENT REYNOLDS NUMBERS

$\frac{x}{h}/N_{Re}$	$u_{\ell}(N_{Re} = 10)$	$u_{\ell}(N_{Re} = 1000)$
0.000	1.0	1.0
.015	.9956	.9952
.02	.9846	.9840
.025	.9665	.9664
.03	.9432	.9437
.04	.8887	.8866
.05	.8318	.8276
.06	.7764	.7689
.08	.6761	.6644
.10	.5918	.5878
.15	.4418	.4398
.20	.3485	.3499
.30	.2427	.2447
.40	.1852	.1874
.60	.1252	.1273

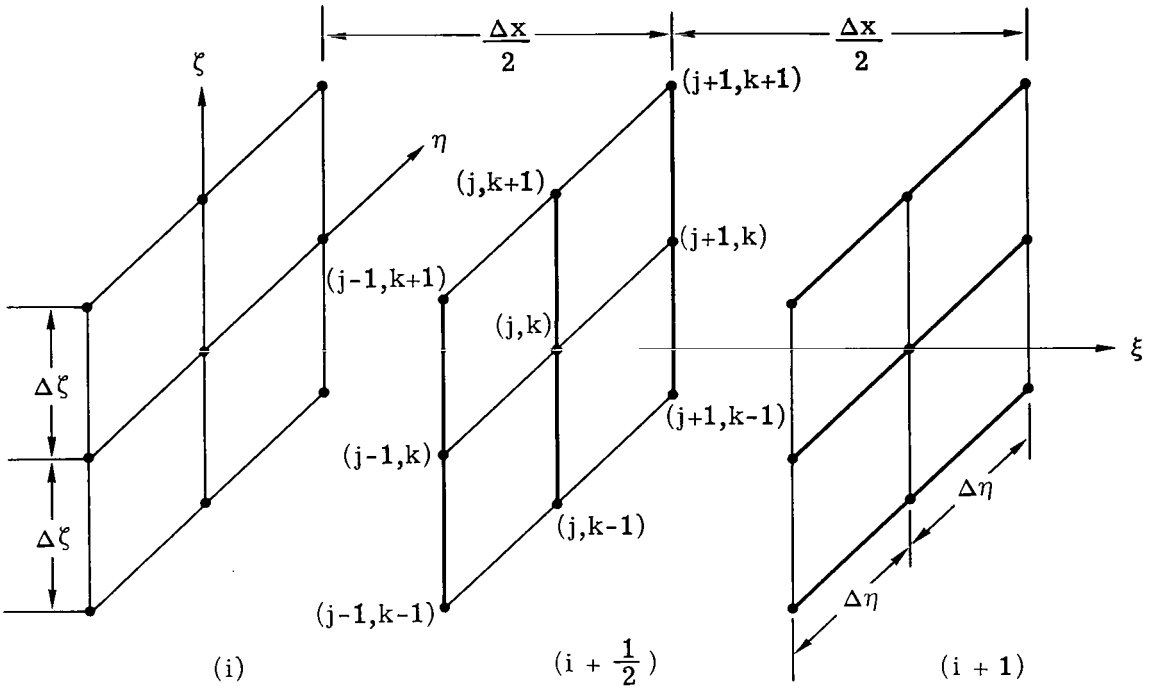

Figure 1.- The ADI procedure: first step implicit in ζ, explicit in η; second step implicit in η, explicit in ζ.

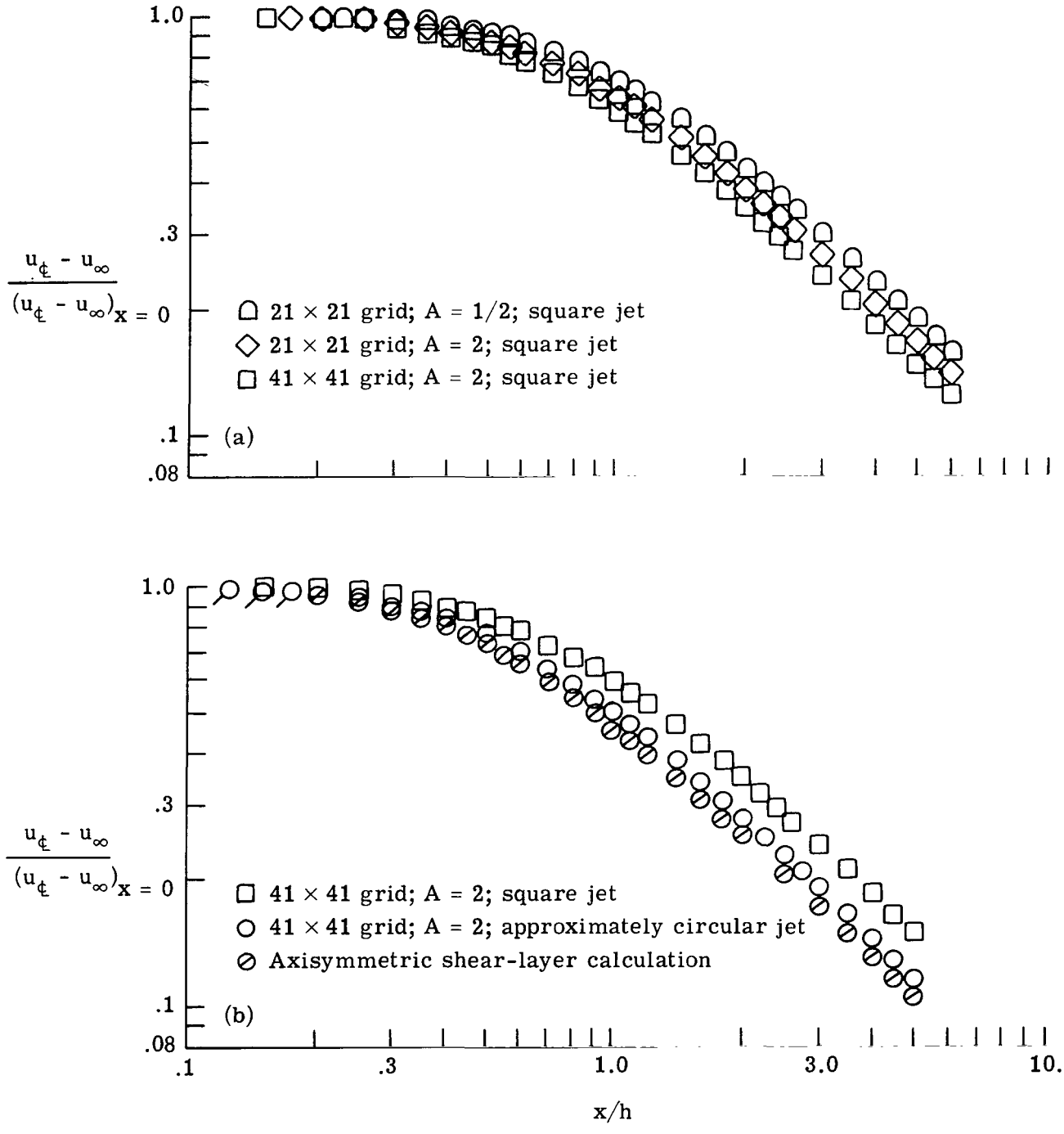

Figure 2.- Streamwise center-line velocity decay for square and axisymmetric jets. $N_{Re} = 10$; $M_{\infty} = 1.2$; $M_j = 1.8$. Flags denote superimposed values.

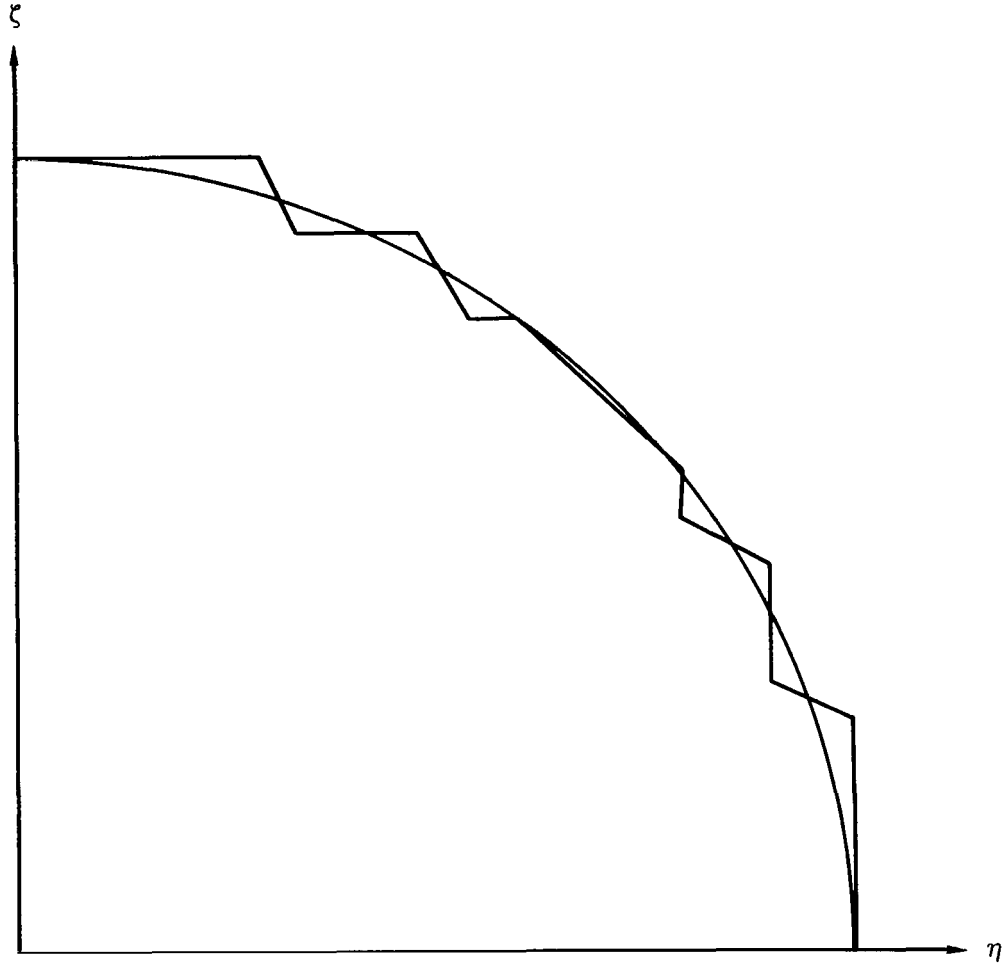

Figure 3.- Approximation to a circle constructed on a Cartesian grid.

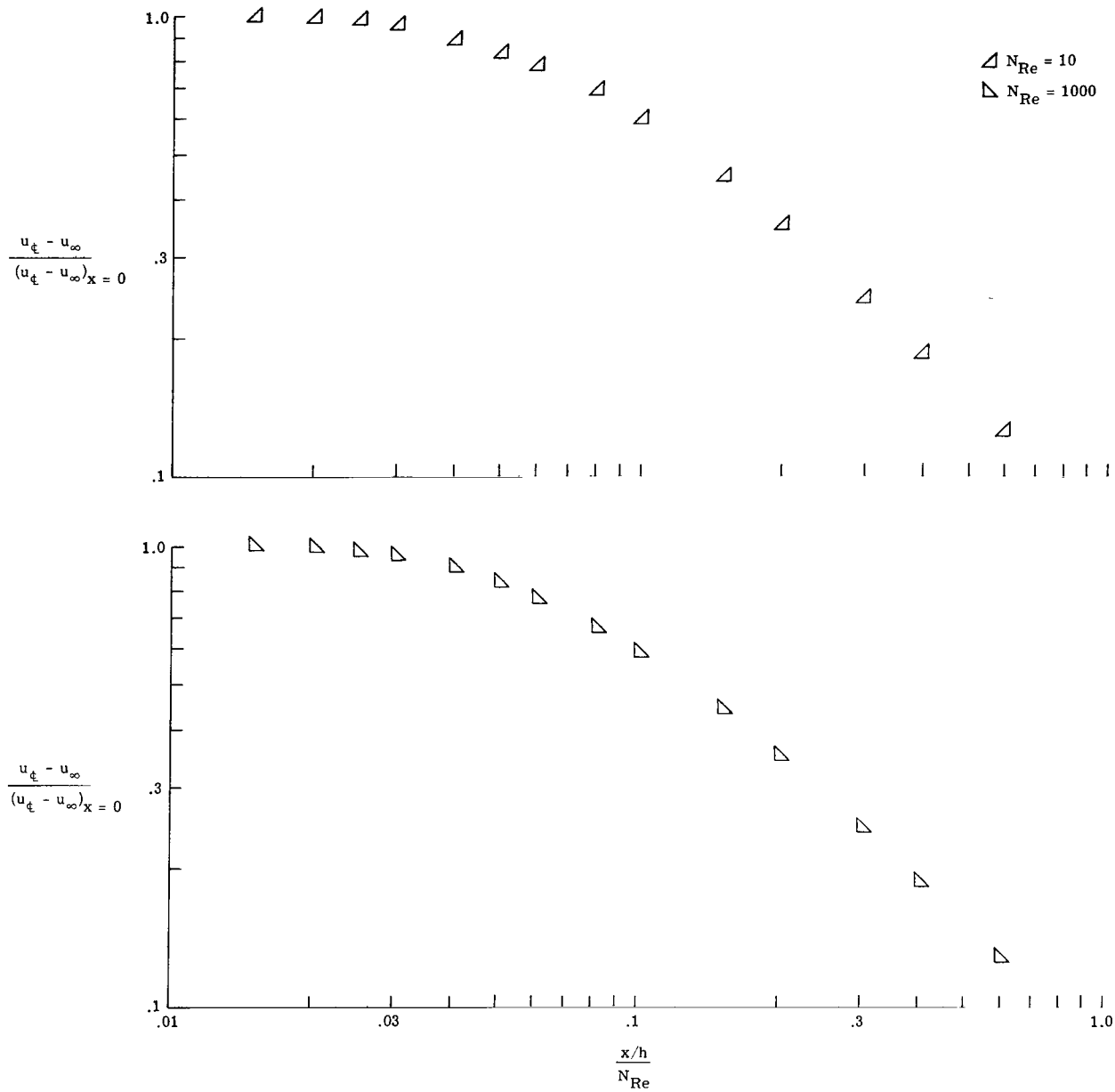

Figure 4.- Reynolds number scaling comparison of center-line velocity decay. $N_{Re} = 10$ and $N_{Re} = 1000$. $M_j = 1.8$.

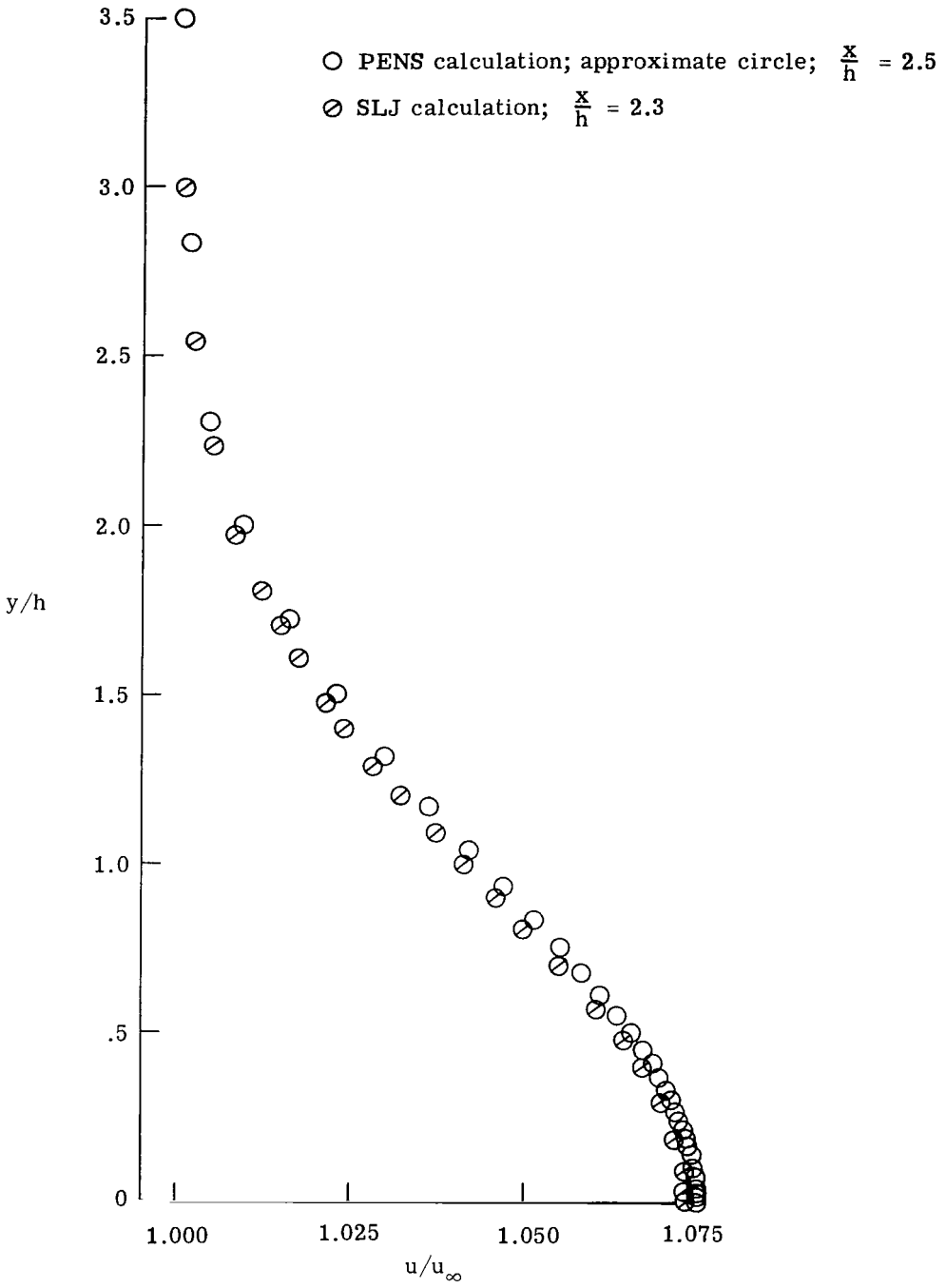

Figure 5.- Streamwise velocity profiles for PENS and SLJ calculations. $N_{Re} = 10$; $M_\infty = 1.2$; and $M_j = 1.8$.

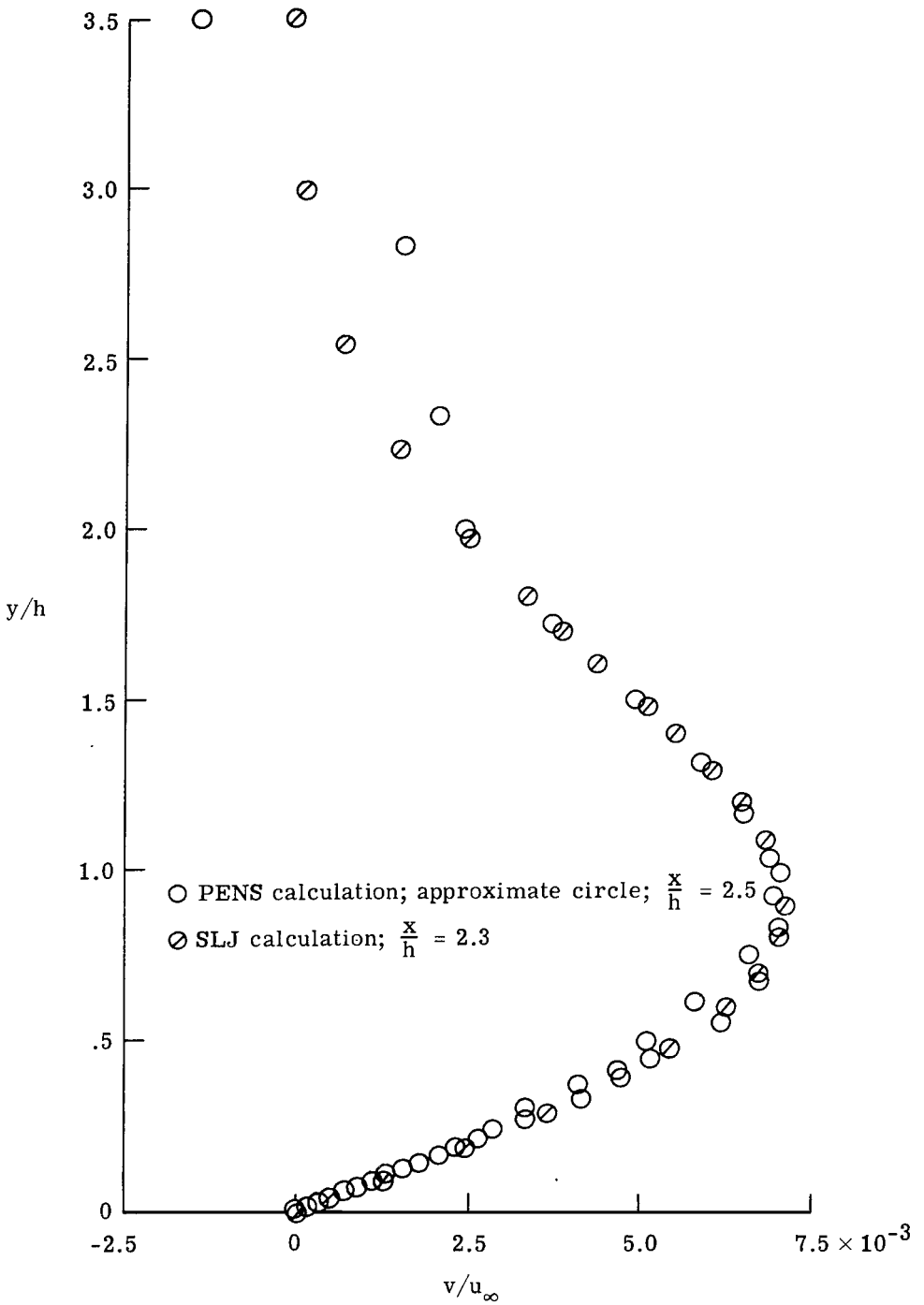

Figure 6.- Normal velocity profiles for PENS and SLJ calculations. N_{Re} = 10; M_∞ = 1.2; and M_j = 1.8.

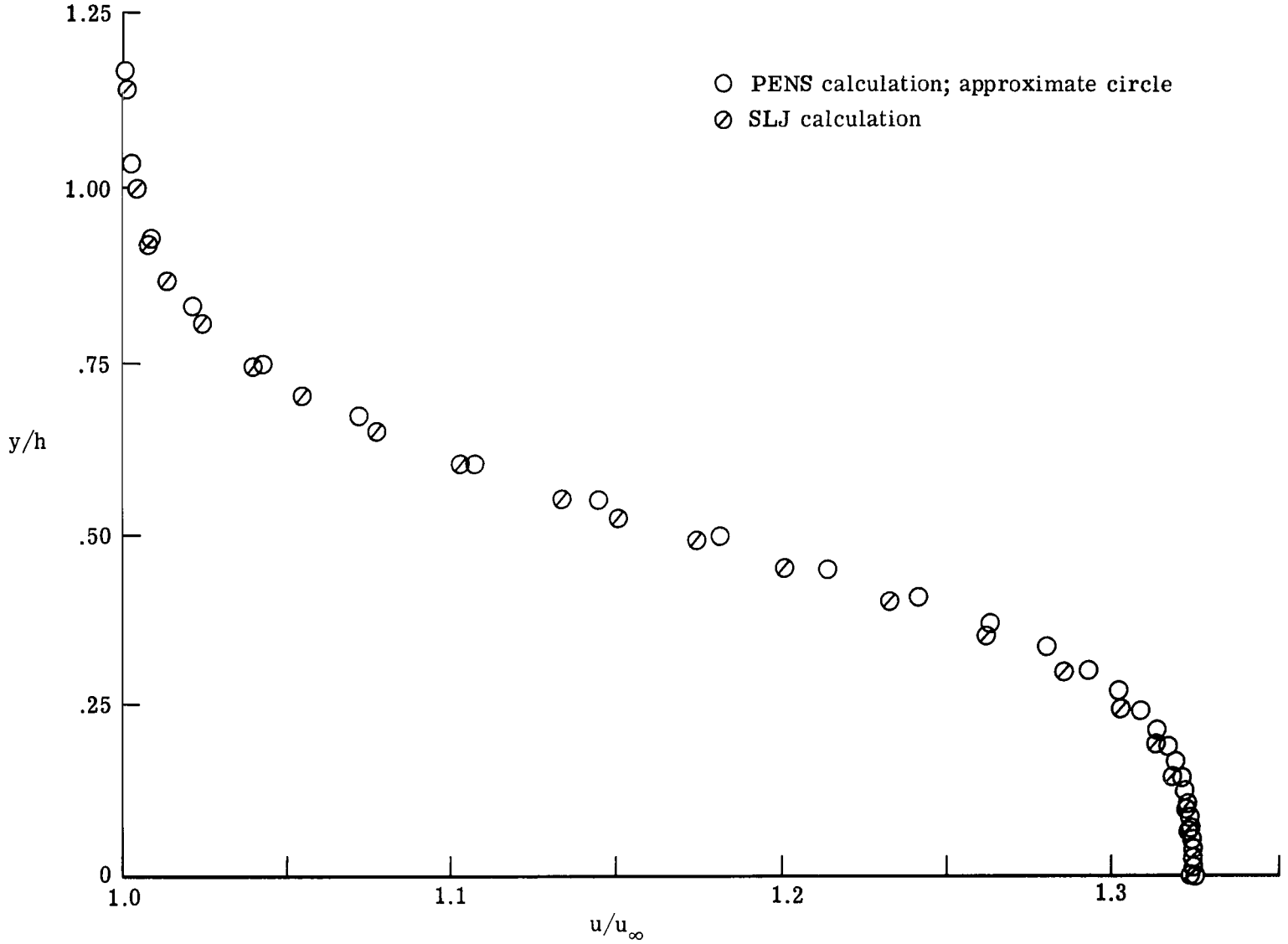

Figure 7.- Streamwise velocity profiles for PENS and SLJ calculations at $x/h = 0.13$. $N_{Re} = 10$; $M_\infty = 1.2$; and $M_j = 1.8$.

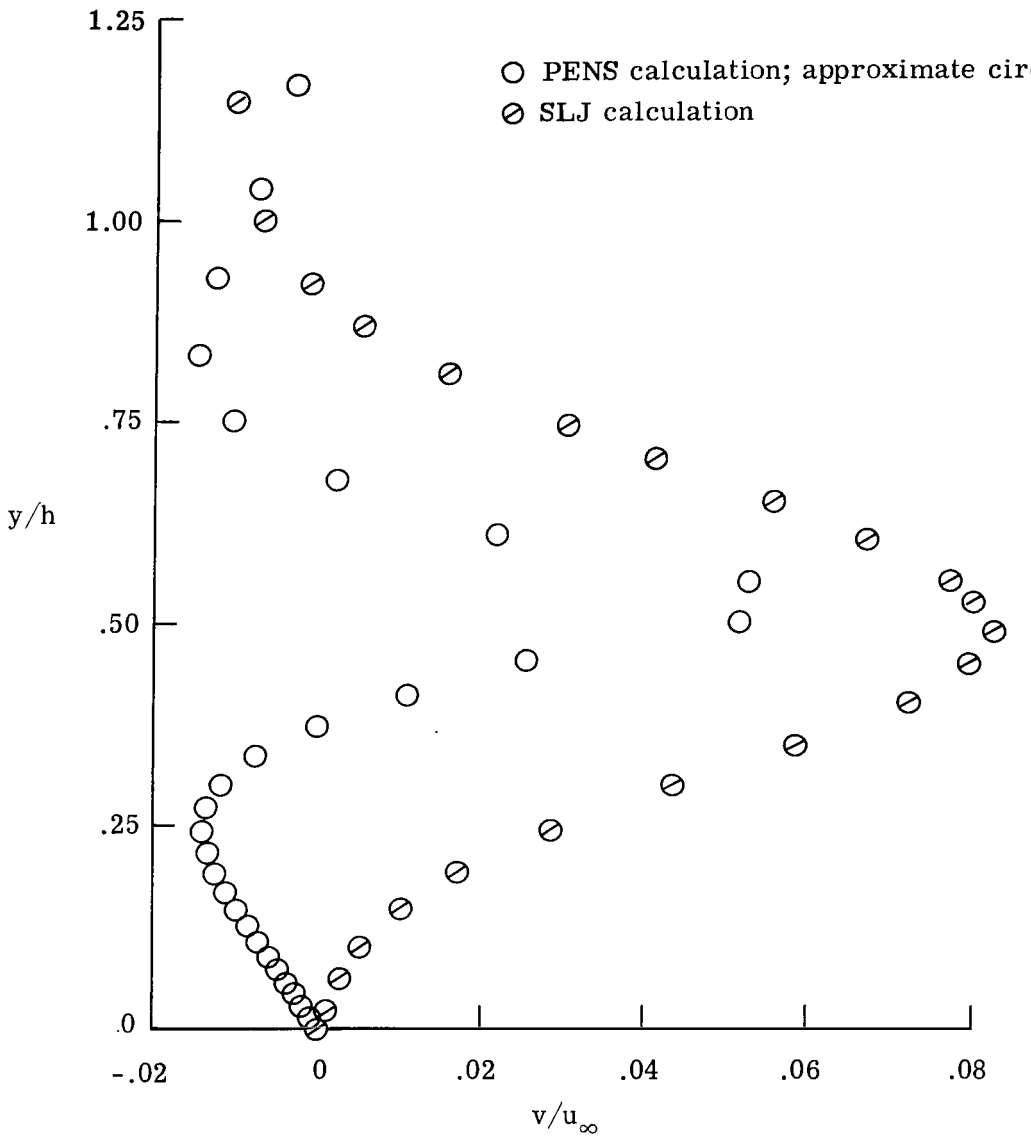

Figure 8.- Normal velocity profiles for PENS and SLJ calculations at $x/h = 0.13$. $N_{Re} = 10$; $M_\infty = 1.2$; and $M_j = 1.8$.

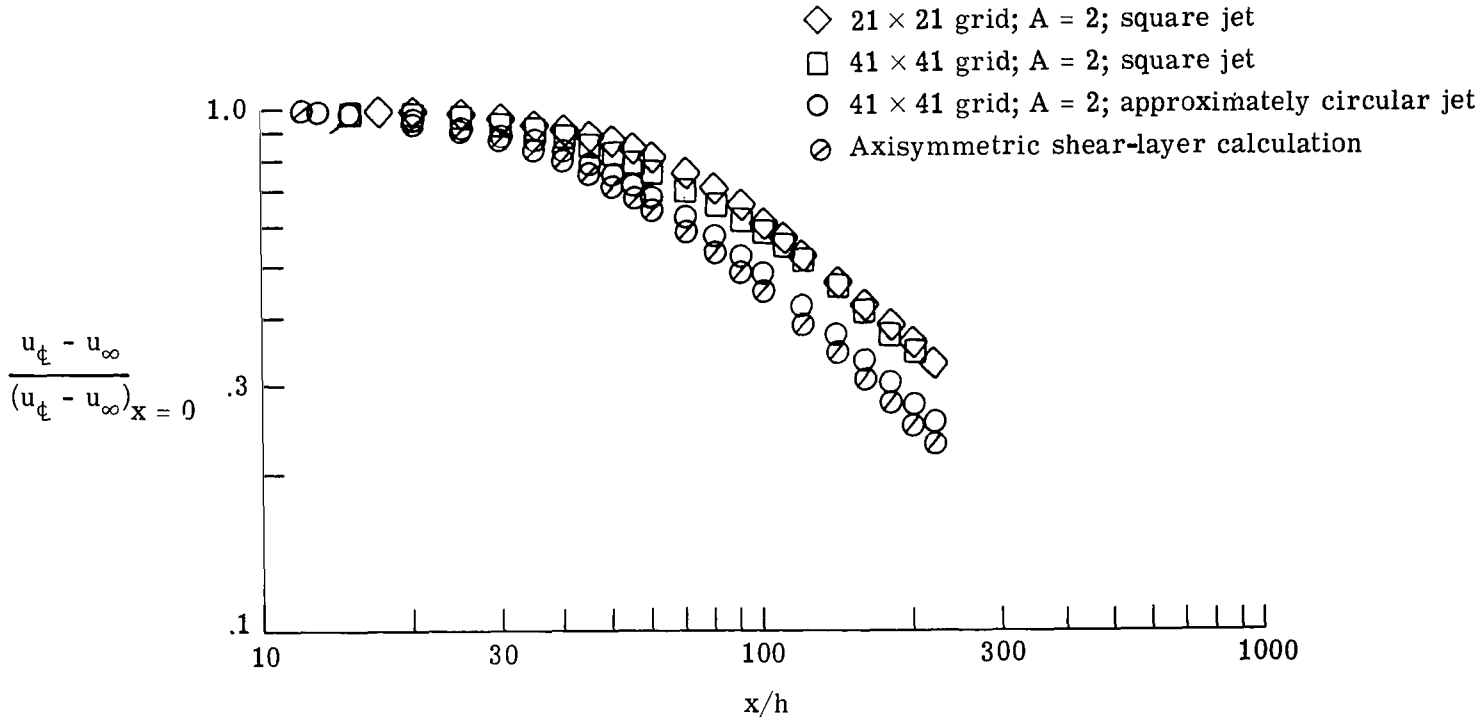

Figure 9.- Streamwise center-line velocity decay for square and axisymmetric jets. N_{Re} = 1000; M_{∞} = 1.2; and M_j = 1.8. Flagged symbol denotes superimposed values.

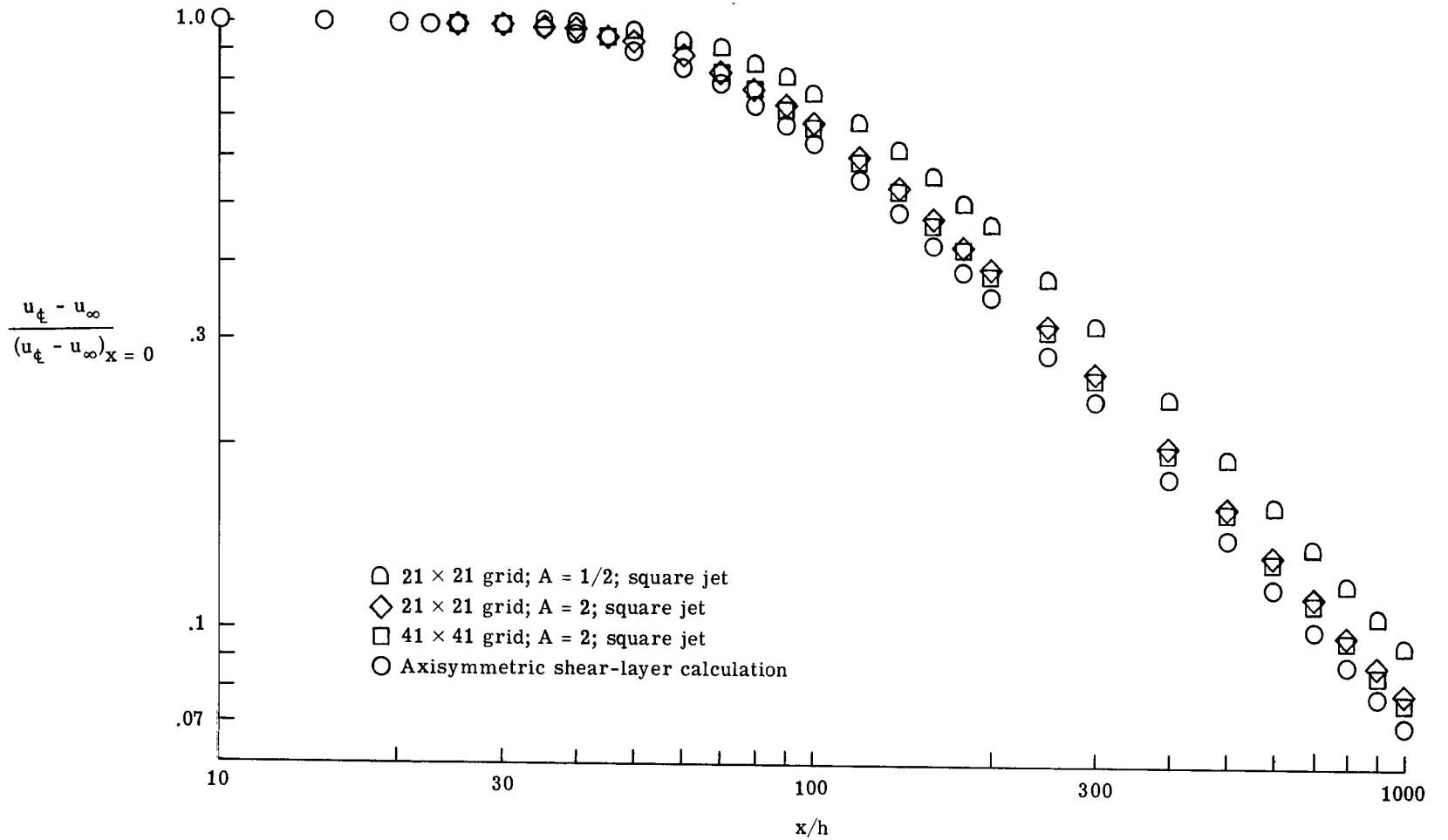

Figure 10.- Streamwise center-line velocity decay for square and axisymmetric jets. $N_{Re} = 1000$; $M_{\infty} = 5.0$; and $M_j = 7.5$.

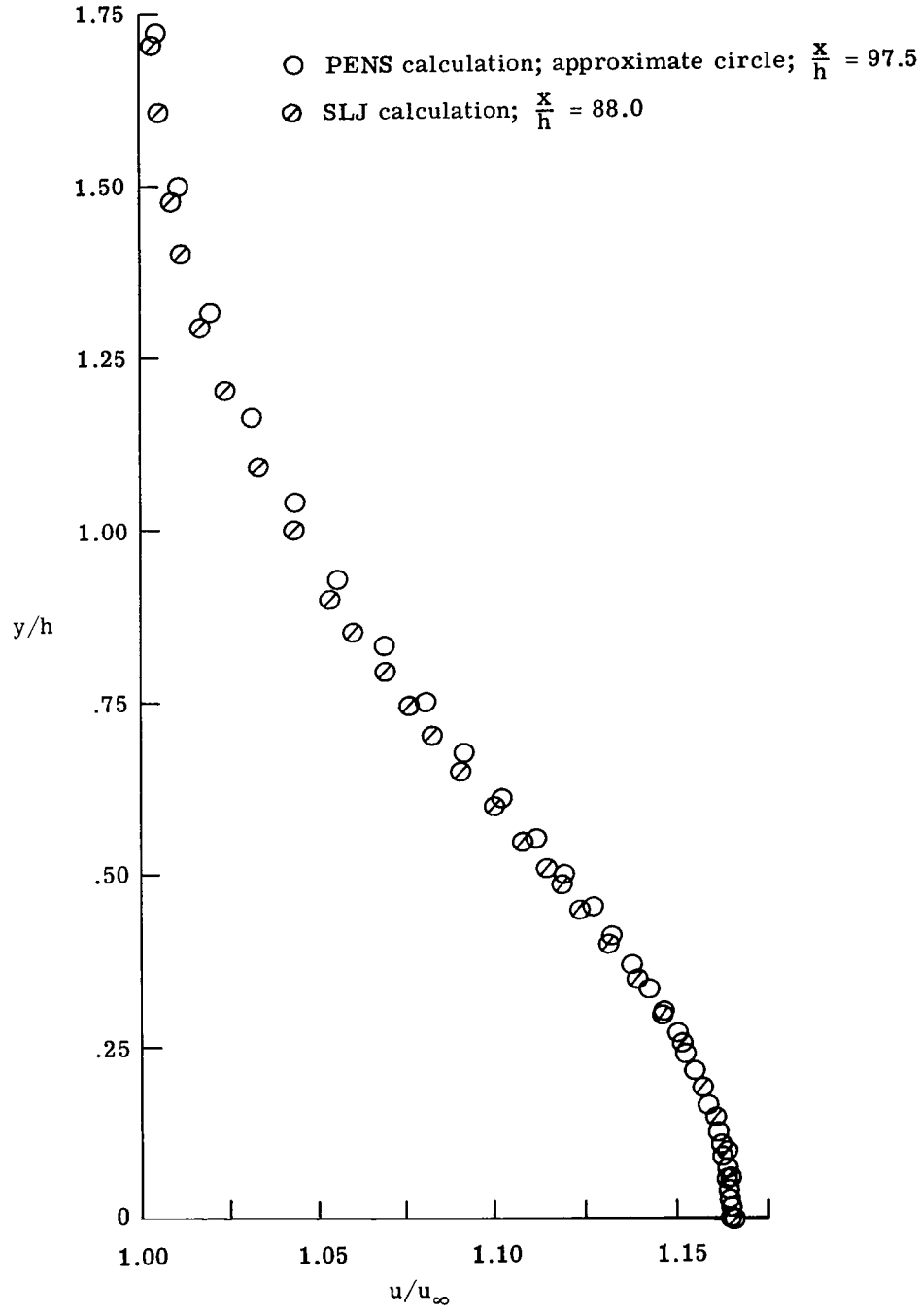

Figure 11.- Streamwise velocity profiles for PENS and SLJ calculations. N_{Re} = 1000; M_∞ = 1.2; and M_j = 1.8.

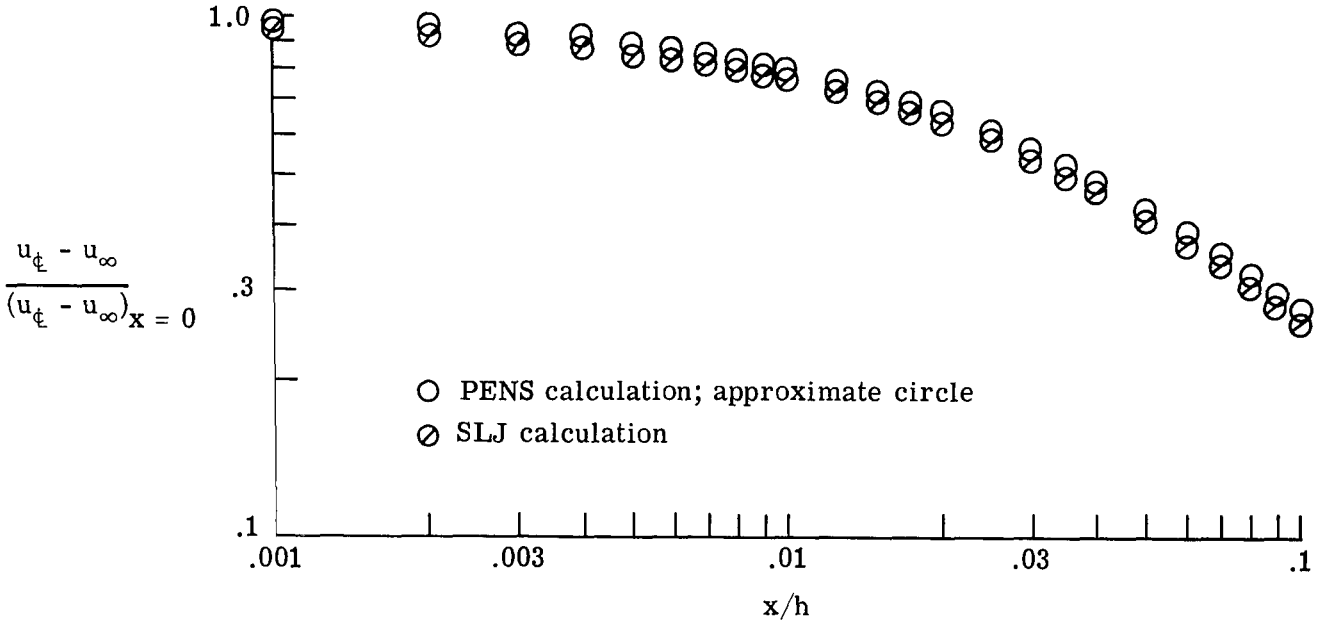

Figure 12.- Streamwise center-line velocity decay for axisymmetric jets started with smooth initial profiles. $N_{Re} = 10$; $M_\infty = 1.2$; and $M_j = 1.8$.

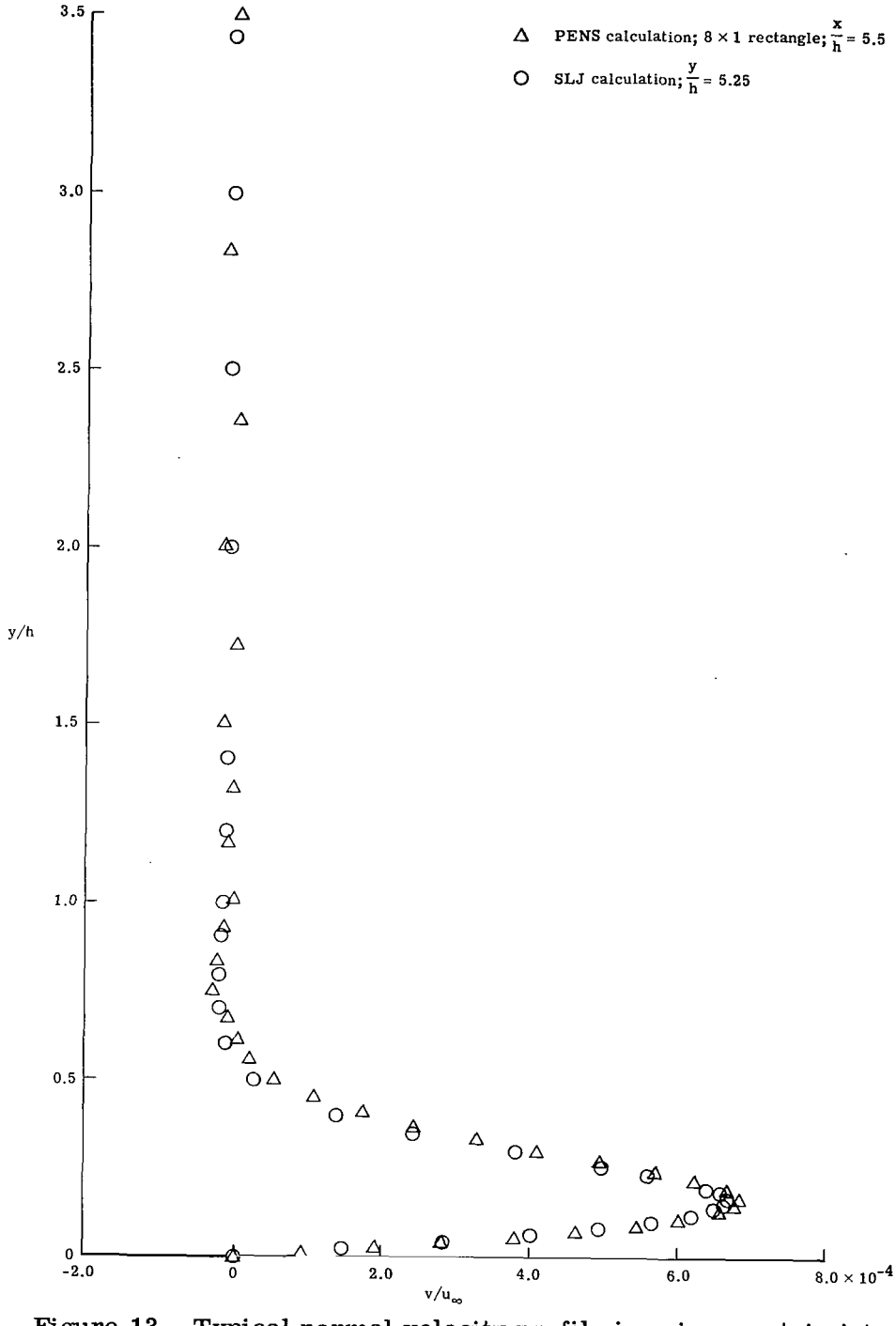

Figure 13.- Typical normal velocity profile in axisymmetric jet calculated using PENS procedure with smooth initial data. N_{Re} = 1000; M_∞ = 1.2; and M_j = 1.8.

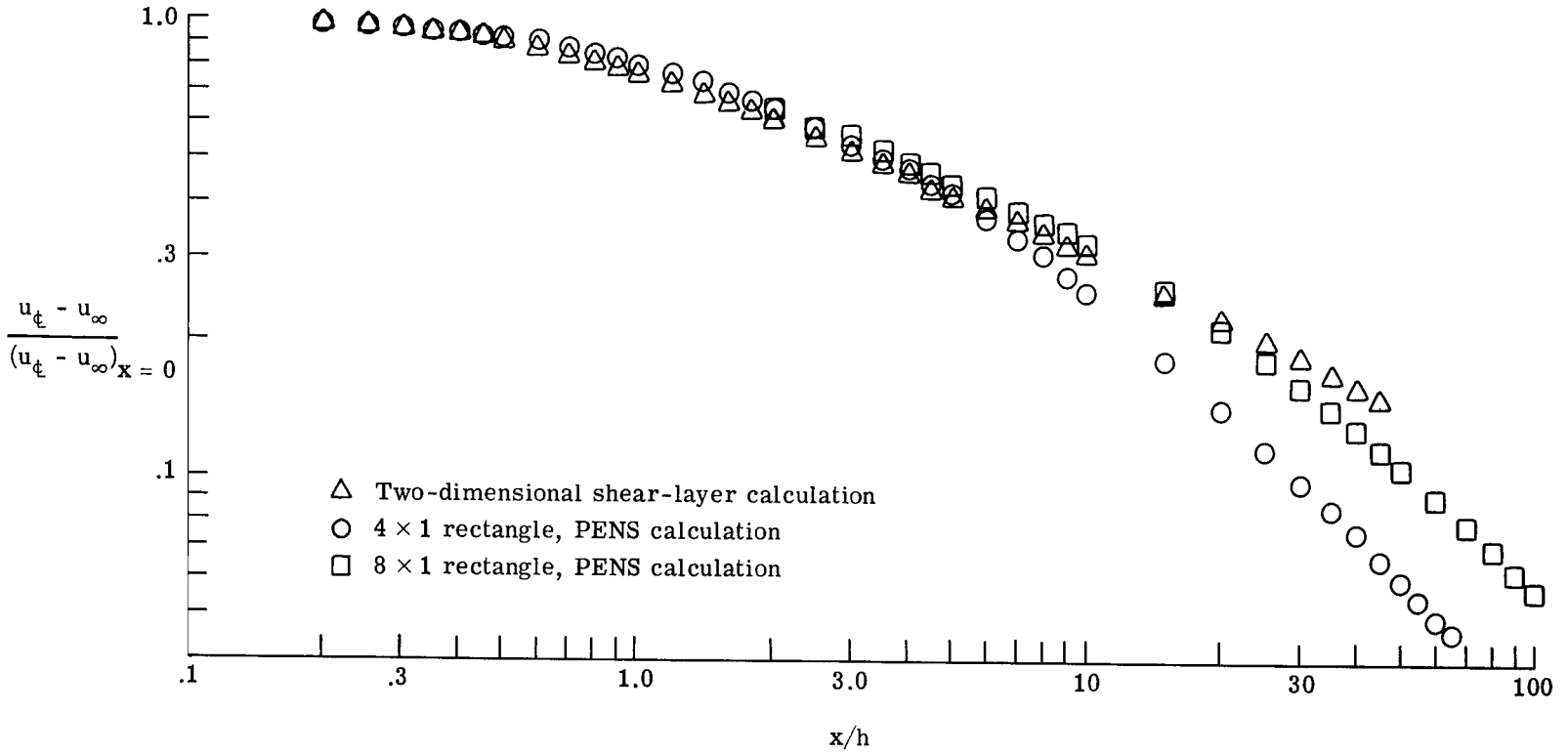

Figure 14.- Streamwise center-line velocity decay for rectangular and two-dimensional jets. $N_{Re} = 10$; $M_{\infty} = 1.2$; and $M_j = 1.8$.

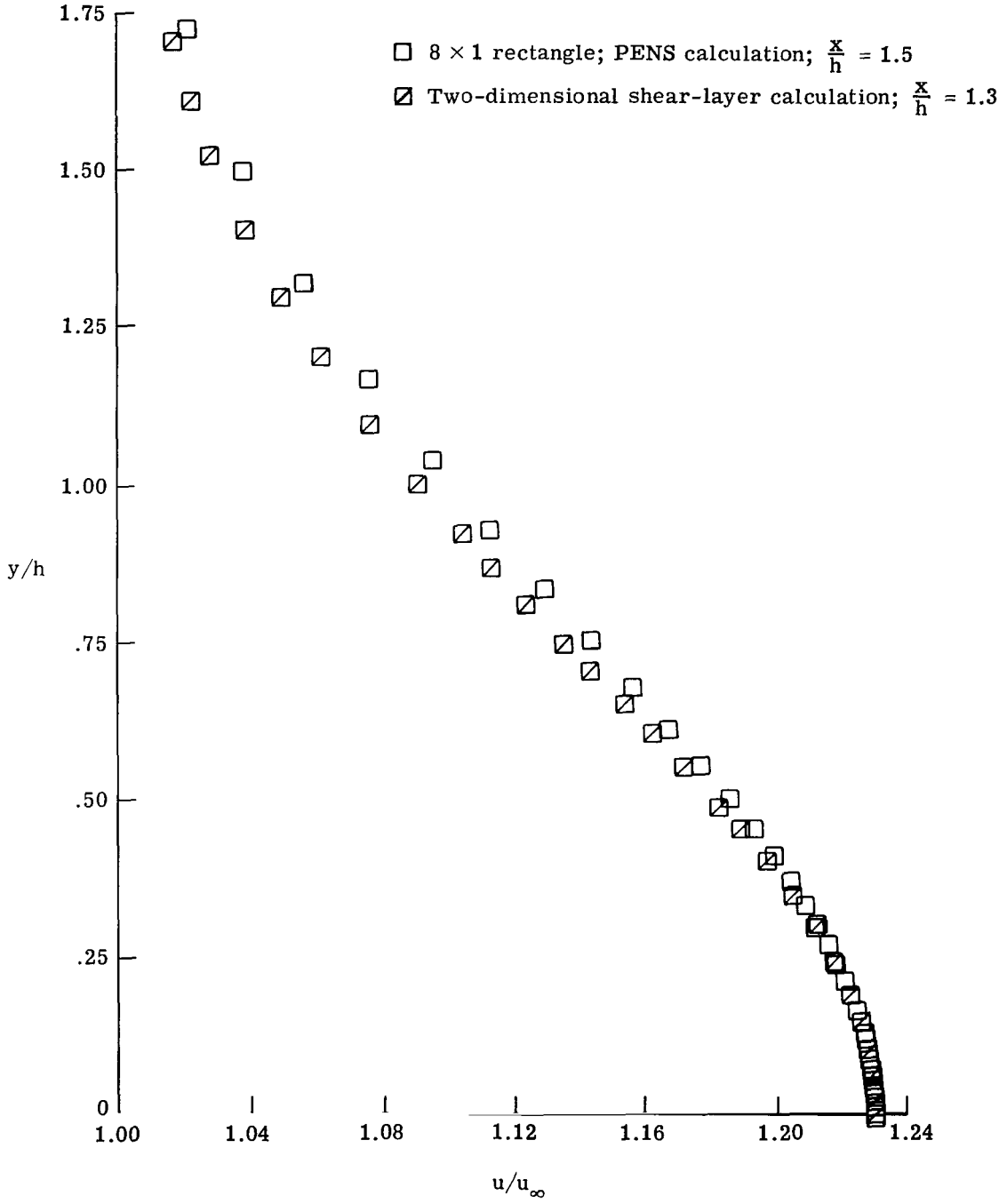

Figure 15.- Streamwise velocity profiles for PENS and SLJ calculations. N_{Re} = 10; M_∞ = 1.2; and M_j = 1.8.

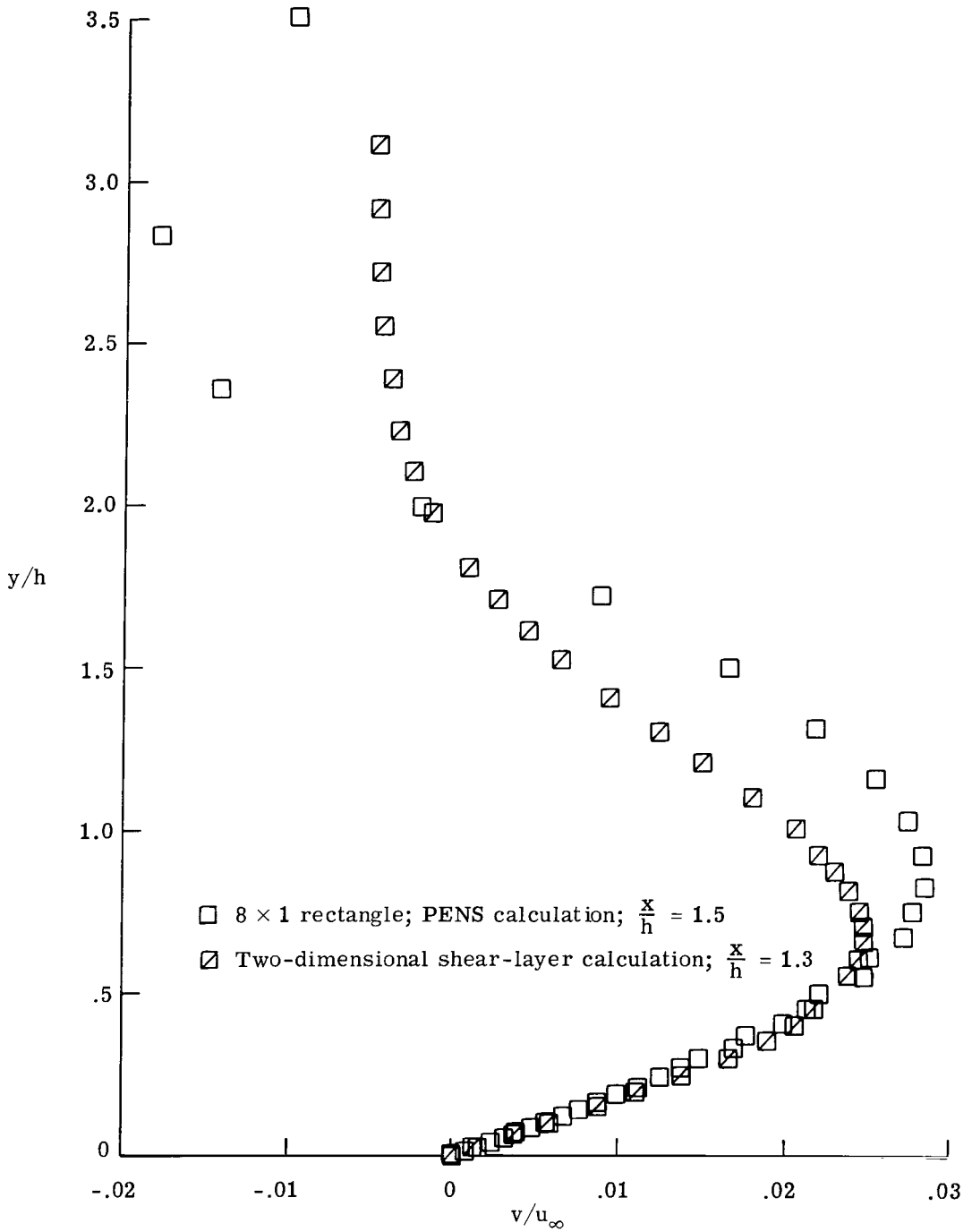

Figure 16.- Normal velocity profiles for PENS and SLJ calculations. N_{Re} = 10; M_∞ = 1.2; and M_j = 1.8.

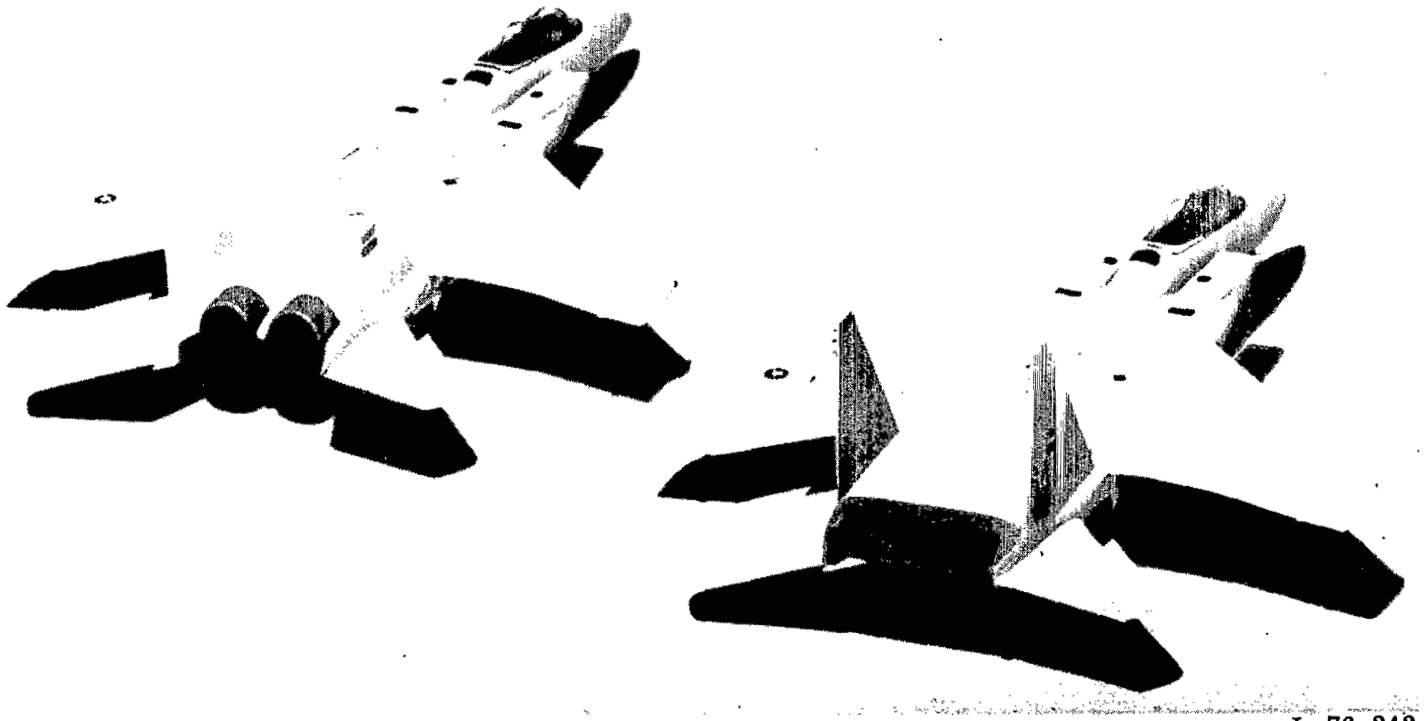

L-76-242

Figure 17.- Current F-15 configuration and proposed modification with two-dimensional nozzles.

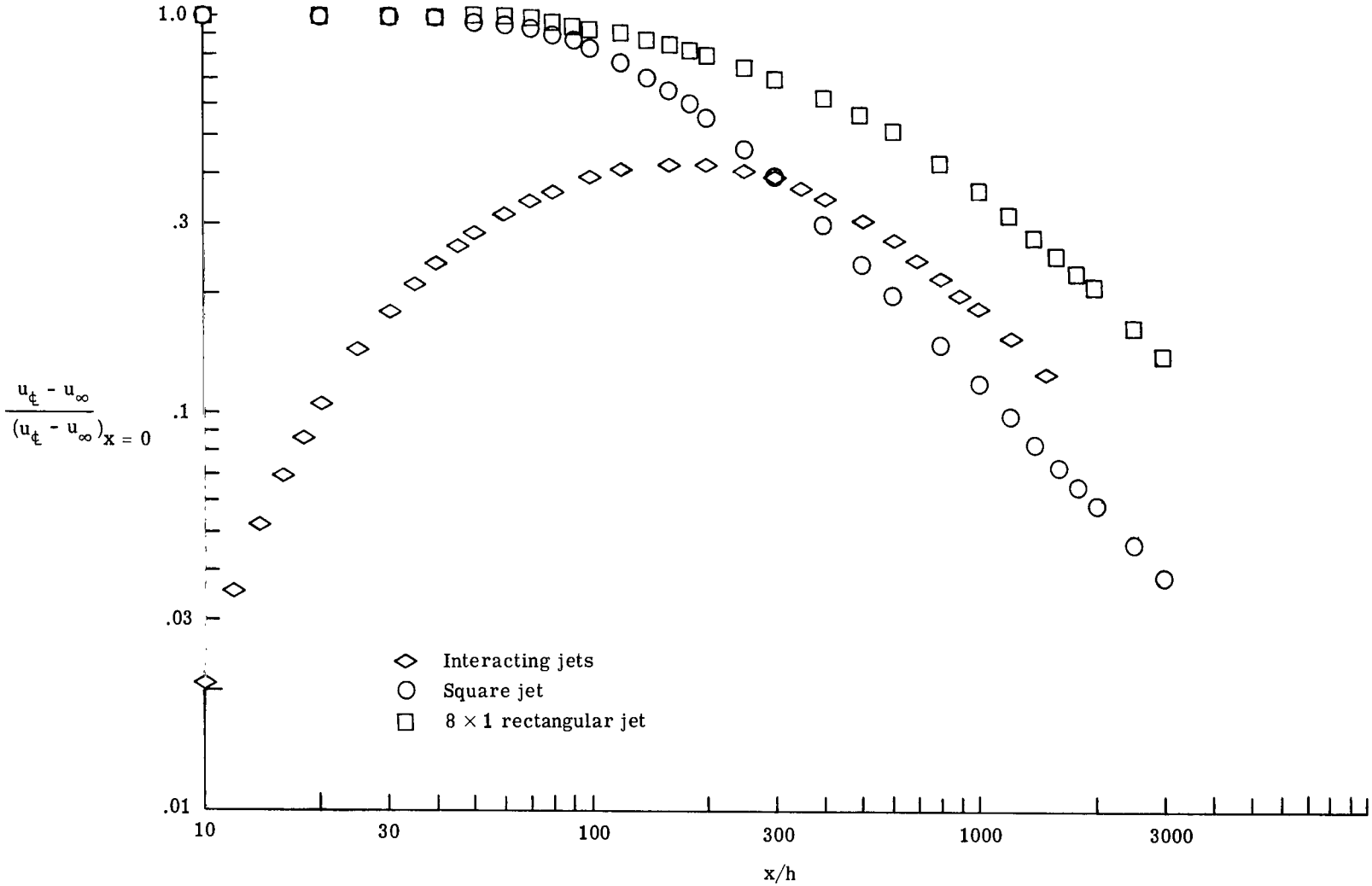

Figure 18.- Streamwise center-line velocity decay for interacting jets. Square and rectangular jets shown for comparison.

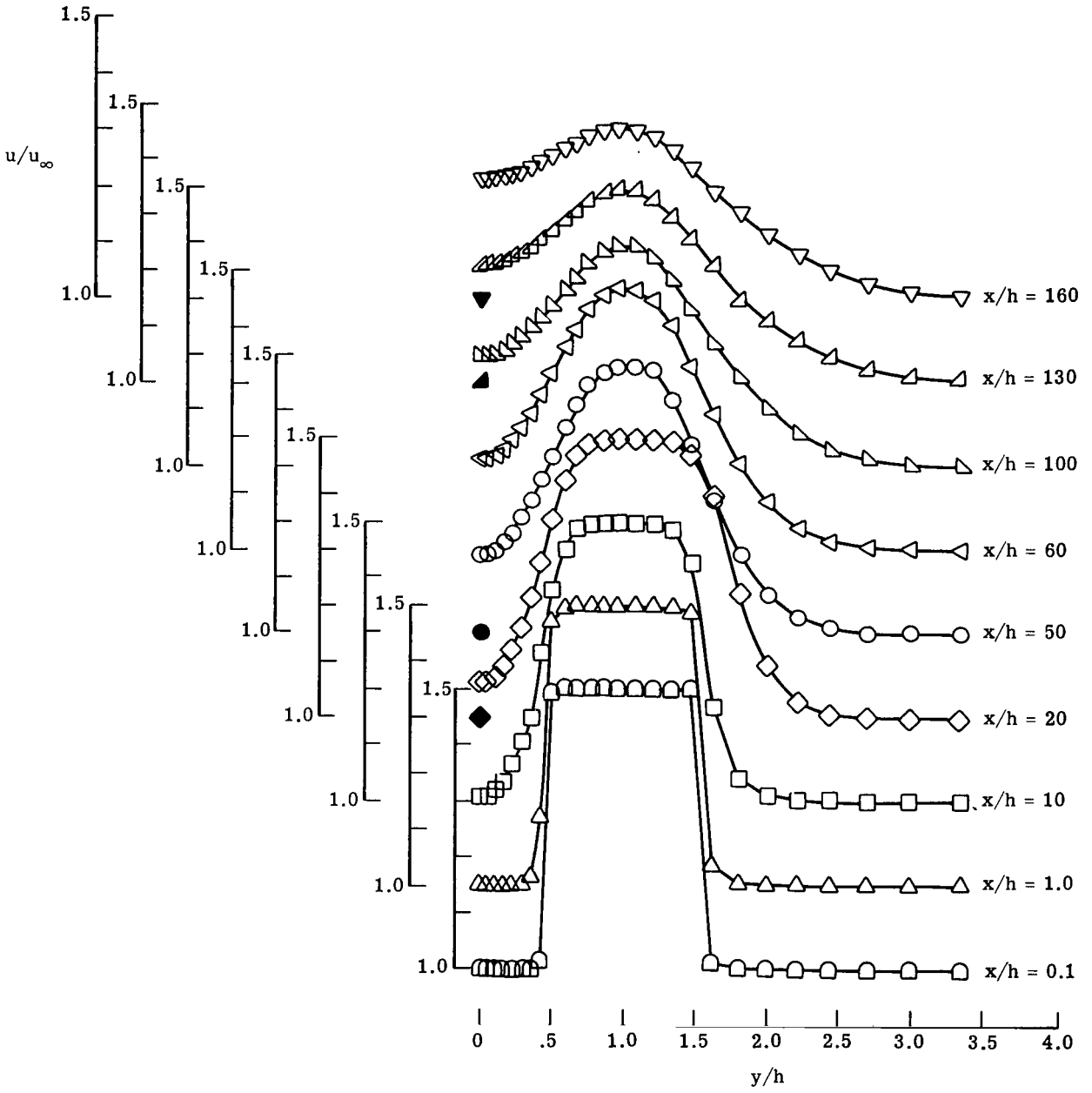

Figure 19.- Streamwise velocity profiles of interacting jets at various x-stations. Solid symbols represent initial center-line velocity level.

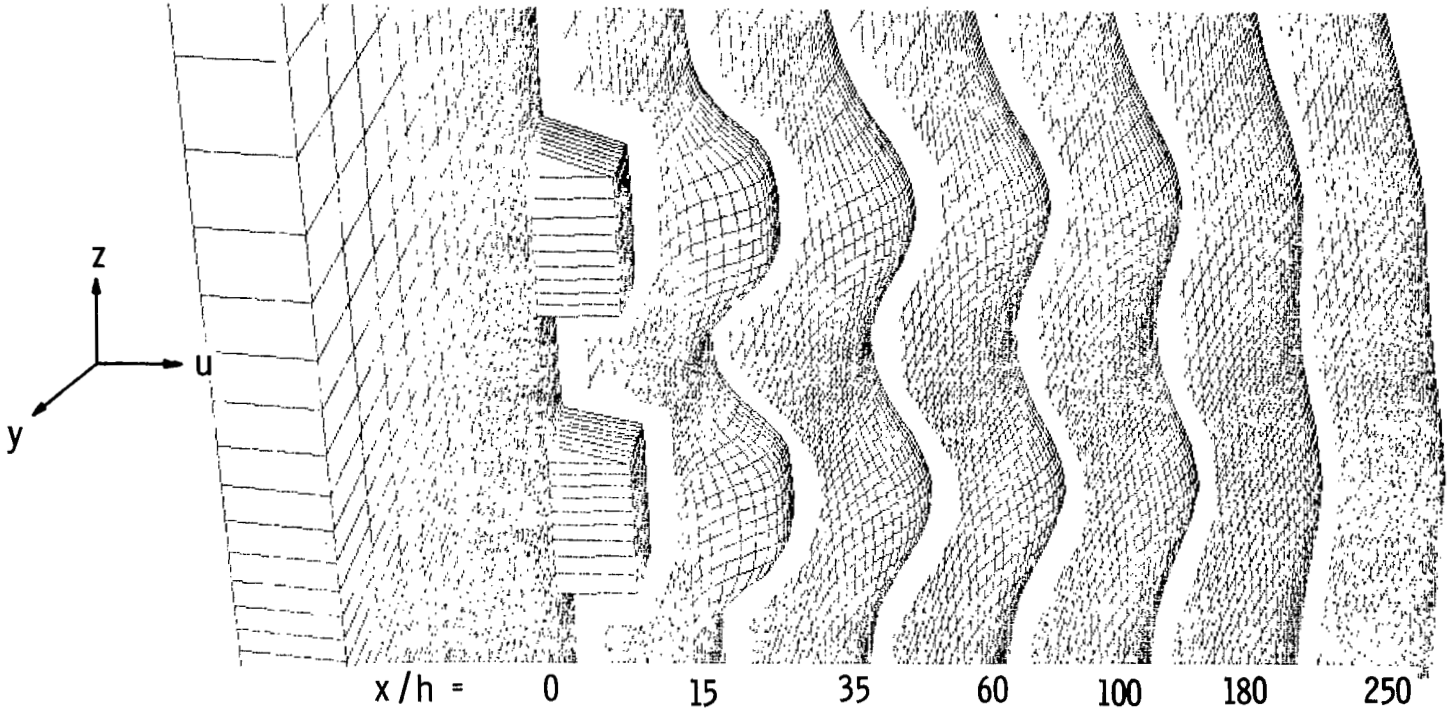

Figure 20.- Perspective plots of interacting jet streamwise velocity at various x-stations.

NASA-Langley, 1976 L-10750

"The aeronautical and space activities of the United States shall be conducted so as to contribute . . . to the expansion of human knowledge of phenomena in the atmosphere and space. The Administration shall provide for the widest practicable and appropriate dissemination of information concerning its activities and the results thereof."

—NATIONAL AERONAUTICS AND SPACE ACT OF 1958

NASA SCIENTIFIC AND TECHNICAL PUBLICATIONS

TECHNICAL REPORTS: Scientific and technical information considered important, complete, and a lasting contribution to existing knowledge.

TECHNICAL NOTES: Information less broad in scope but nevertheless of importance as a contribution to existing knowledge.

TECHNICAL MEMORANDUMS: Information receiving limited distribution because of preliminary data, security classification, or other reasons. Also includes conference proceedings with either limited or unlimited distribution.

CONTRACTOR REPORTS: Scientific and technical information generated under a NASA contract or grant and considered an important contribution to existing knowledge.

TECHNICAL TRANSLATIONS: Information published in a foreign language considered to merit NASA distribution in English.

SPECIAL PUBLICATIONS: Information derived from or of value to NASA activities. Publications include final reports of major projects, monographs, data compilations, handbooks, sourcebooks, and special bibliographies.

TECHNOLOGY UTILIZATION PUBLICATIONS: Information on technology used by NASA that may be of particular interest in commercial and other non-aerospace applications. Publications include Tech Briefs, Technology Utilization Reports and Technology Surveys.

Details on the availability of these publications may be obtained from:

SCIENTIFIC AND TECHNICAL INFORMATION OFFICE

NATIONAL AERONAUTICS AND SPACE ADMINISTRATION

Washington, D.C. 20546